Report No. NADC-90001-60

PREDICTION OF FIBER/MATRIX INTERPHASE PROPERTIES AND THEIR INFLUENCE ON INTERFACE STRESS, DISPLACEMENT AND FRACTURE TOUGHNESS OF COMPOSITE MATERIAL

Hsi Chin Tsai, Annete M. Arocho, and Lee W. Gause
Air Vehicle and Crew Systems Technology Department (Code 6043)
NAVAL AIR DEVELOPMENT CENTER
Warminster, PA 18974-5000

3 JANUARY 1990

DTIC

Unclassified

REPORT DOCUMENTATION PAGE		Form Approved OMB No 0704-0188

1a REPORT SECURITY CLASSIFICATION	1b RESTRICTIVE MARKINGS
Unclassified	

2a SECURITY CLASSIFICATION AUTHORITY	3 DISTRIBUTION/AVAILABILITY OF REPORT
	Approved for Public Release;
2b DECLASSIFICATION/DOWNGRADING SCHEDULE	Distribution is Unlimited

4 PERFORMING ORGANIZATION REPORT NUMBER(S)	5 MONITORING ORGANIZATION REPORT NUMBER(S)
NADC-90001-60	

6a NAME OF PERFORMING ORGANIZATION	6b OFFICE SYMBOL (If applicable)	7a NAME OF MONITORING ORGANIZATION
Air Vehicle Crew Systems Technology Department	6043	

6c ADDRESS (City, State, and ZIP Code)	7b ADDRESS (City, State, and ZIP Code)
NAVAL AIR DEVELOPMENT CENTER Warminster, PA 18974-5000	

8a NAME OF FUNDING/SPONSORING ORGANIZATION	8b OFFICE SYMBOL (If applicable)	9 PROCUREMENT INSTRUMENT IDENTIFICATION NUMBER
OFFICE OF NAVAL RESEARCH		

8c ADDRESS (City, State, and ZIP Code)	10 SOURCE OF FUNDING NUMBERS			
Washington, DC 20350	PROGRAM ELEMENT NO	PROJECT NO	TASK NO	WORK UNIT ACCESSION NO
	0601153N		R0220400A	108634

11 TITLE (Include Security Classification)
Prediction Of Fiber/Matrix Interphase Properties And Their Influence On Interface Stress, Displacement And Fracture Toughness Of Composite Material

12 PERSONAL AUTHOR(S)
Hsi Chin Tsai, Annete M. Arocho, and Lee W. Gause

13a TYPE OF REPORT	13b TIME COVERED	14 DATE OF REPORT (Year, Month, Day)	15 PAGE COUNT
Phase	FROM 10/88 TO 10/89	1990 January 3	49

16 SUPPLEMENTARY NOTATION

17 COSATI CODES			18 SUBJECT TERMS (Continue on reverse if necessary and identify by block number)
FIELD	GROUP	SUB-GROUP	Fiber/Matrix Interface, Interphase, Interphase Properties, Fracture Toughness, Organic Composites
11	04		

19 ABSTRACT (Continue on reverse if necessary and identify by block number)

An elastic shear lag analysis, which includes an interphase region, has been developed and correlated with Mandell's micro-debonding test data [1] to determine the thickness and material properties of the interphase. The shear strength and the relationship between thickness and shear modulus of interphase were determined for both glass/epoxy and graphite/epoxy composites.

An axisymmetric finite element model, which includes the interphase properties obtained from the shear lag analysis, was also developed. The effects of the interphase on stresses and deformation at the interface and fracture toughness of the fibrous composites were investigated. The following conclusions were drawn from the study:
(1) By including an interphase, both the shear lag analysis and finite element model provide very good predictions. (2) An interphase exists and is softer than the matrix. (3) The interphase has significant effect on stress concentration, displacement and

20 DISTRIBUTION AVAILABILITY OF ABSTRACT	21 ABSTRACT SECURITY CLASSIFICATION
☐ UNCLASSIFIED UNLIMITED ☐ SAME AS RPT ☒ DTIC USERS	Unclassified

22a NAME OF RESPONSIBLE INDIVIDUAL	22b TELEPHONE (Include Area Code)	22c OFFICE SYMBOL
Hsi Chin Tsai	215-441-2871	6043

DD Form 1473, JUN 86   Previous editions are obsolete   SECURITY CLASSIFICATION OF THIS PAGE

S/N 0102-LF-014-6603   Unclassified

Block 19.

fracture toughness of the fibrous composite.

CONTENTS

FIGURES

TABLES

ACKNOWLEDGEMENTS

INTRODUCTION

The fiber/matrix interface has a significant influence on the structural integrity of a fibrous composite. For example, the stronger the interface bond, the higher the composite's static strength. However, a strong interface bond also yields a brittle and notch-sensitive composite[2] and, on the other hand, a weaker interface results in a higher fracture toughness composite.[2,3]

Conventional methods for predicting the stress at the fiber/matrix interface can be divided into three categories. These are: shear lag theory,[4,5,6] two-dimensional, finite-element analysis,[7,8] and three-dimensional, finite-element analysis.[9] These methods all assume zero interface thickness and uniform, homogeneous matrix properties.

Recently, several researchers have suggested that the volume of material immediately surrounding the fiber is significantly different from the bulk matrix.[10,11,12,13] This volume of material is commonly referred to as the interphase. Drzal[10] has suggested that this material may be more rigid than the bulk matrix. Piggott[11] has found that to explain the Young's moduli of short-fiber composites, the interphase must have a very low modulus, i.e., much softer than the bulk matrix.

No direct evidence has been found for the presence of an interphase in organic matrix composites nor are its properties and dimensions known. The objective of this study is to prove the existence of interphase and to determine interphase elastic properties, if possible. Included in this work is an investigation to determine the influence of interphases on stress at the fiber/matrix interfaces on displacements and on fracture toughnesses of fibrous composites.

SHEAR LAG THEORY WITH DISTINCT INTERPHASE

To include the interphase into a composite-material structural analysis model, material properties and the thickness of the interphase must be known in advance. Experimental data on interphase properties does not exist. One way to deduce the interphase characteristics is to assume initial values for the interphase and then iterate the properties and thickness until analytical results converge to match the corresponding experimentally observable results.

Since the thickness of interphase can be very small compared with the fiber diameter, a very large number of finite elements would be needed if the finite element technique was used for the iteration procedure. This would be time-consuming and costly. A closed-form solution, based upon shear-lag theory, was employed instead.

In the following, a shear lag analysis, which includes and interphase region between the fiber and bulk matrix, has been developed. Mandell's microdebonding test data[1] was used to determine the interphase material properties and thickness.

THEORY

Mandell's microdebonding test,[1] Figure 1, was modeled as shown in Figure 2. Four types of materials were included in this model; namely, fiber, interphase, matrix, and composite. Note that a load is applied at the end of a fiber, and that the material outside the matrix was modeled as equivalent smeared composite material.

By employing the shear lag theory, the following assumptions were made:

(1) Axial load is carried by the fiber alone, while the interphase and matrix carry the shear load only.

LOAD

PROBE
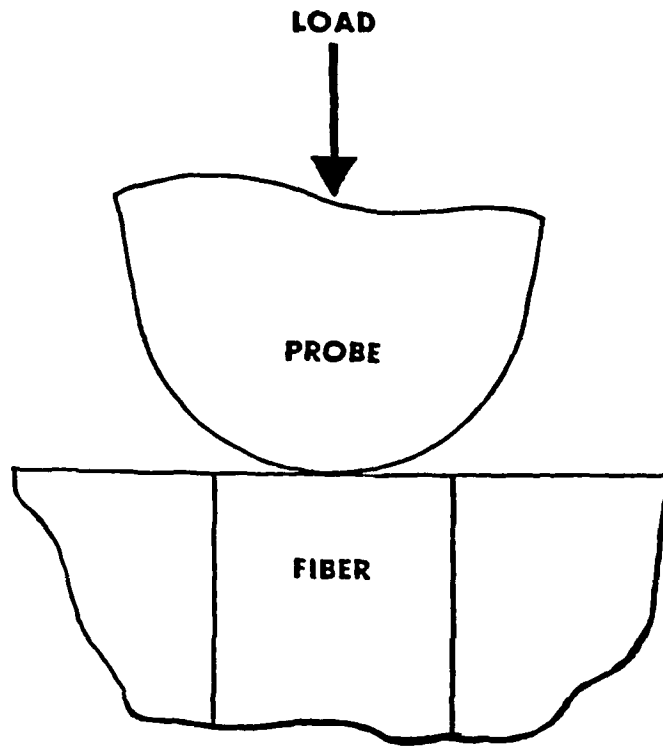
FIBER

Figure 1. Schematic of Loading for Microdebonding Test.
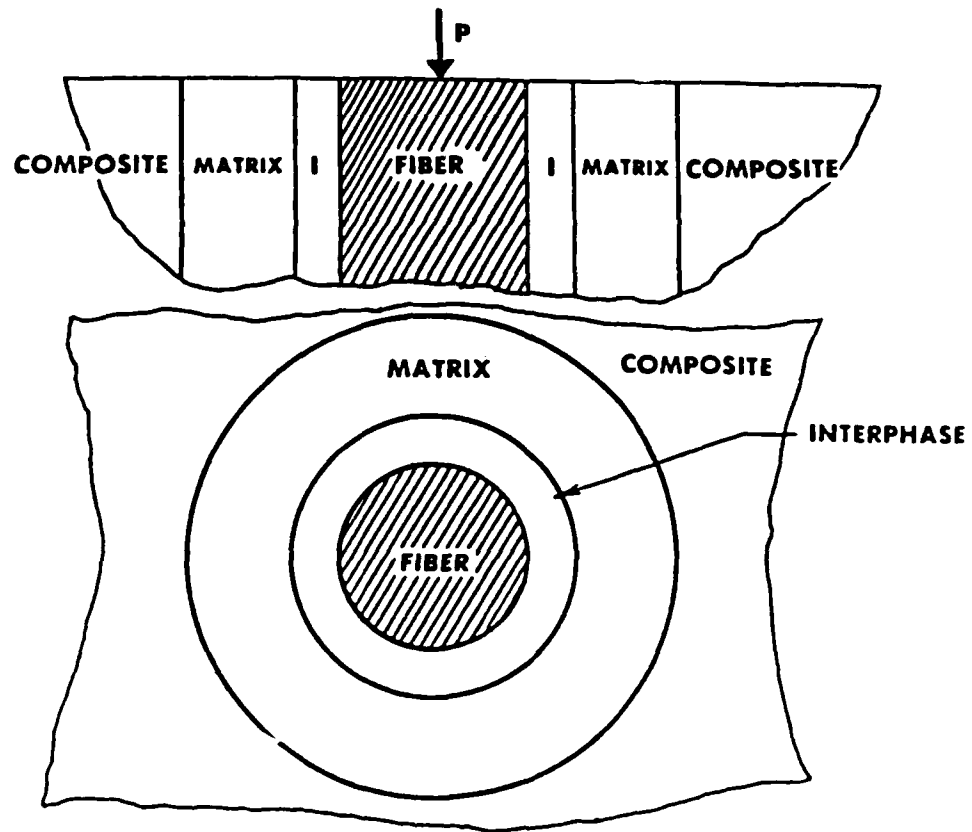
Figure 2. Modeling of Fiber/Matrix Interface.

(2) Fixed boundary conditions apply at the boundary between the matrix and equivalent composite.

The freebody diagrams of the loaded fiber and adjacent interphase and matrix are shown in Figures 3a and 3b. The equilibrium equations are as follows:

$$\frac{dF}{dz} + 2\pi r_i \tau_i = 0 \tag{1}$$

$$\frac{dF}{dz} + 2\pi r_m \tau_m = 0 \tag{2}$$

From equations (1) and (2), we have:

$$\tau_i r_i = r_m \tau_m = r\tau \tag{3}$$

where

F = fiber force at z

r_f, r_i = radius of fiber and interphase, respectively

τ_i, τ_m = shear stress of interphase and matrix, respectively.

From the theory of elasticity and Figure 4:

$$\tau = \frac{dW}{dr} G$$

$$r_F \leq r \leq r_i$$

$$\frac{dW}{dr} = \frac{\tau}{G_i} \tag{4}$$

where τ is the shear stress in the interphase, and G_i is the shear modulus of interphase.

4
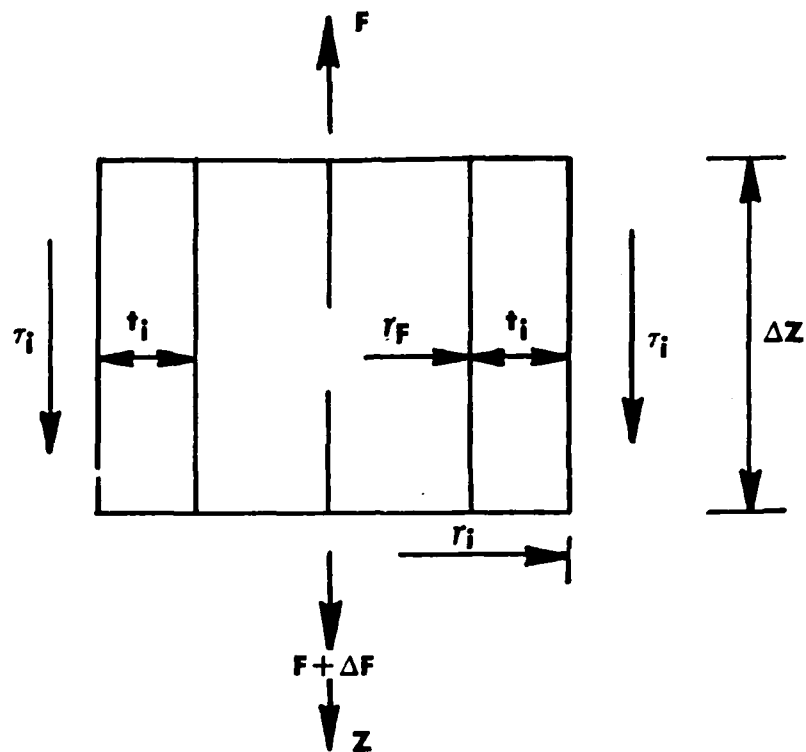
Figure 3a. Free Body Diagram Involving Fiber and Interphase.
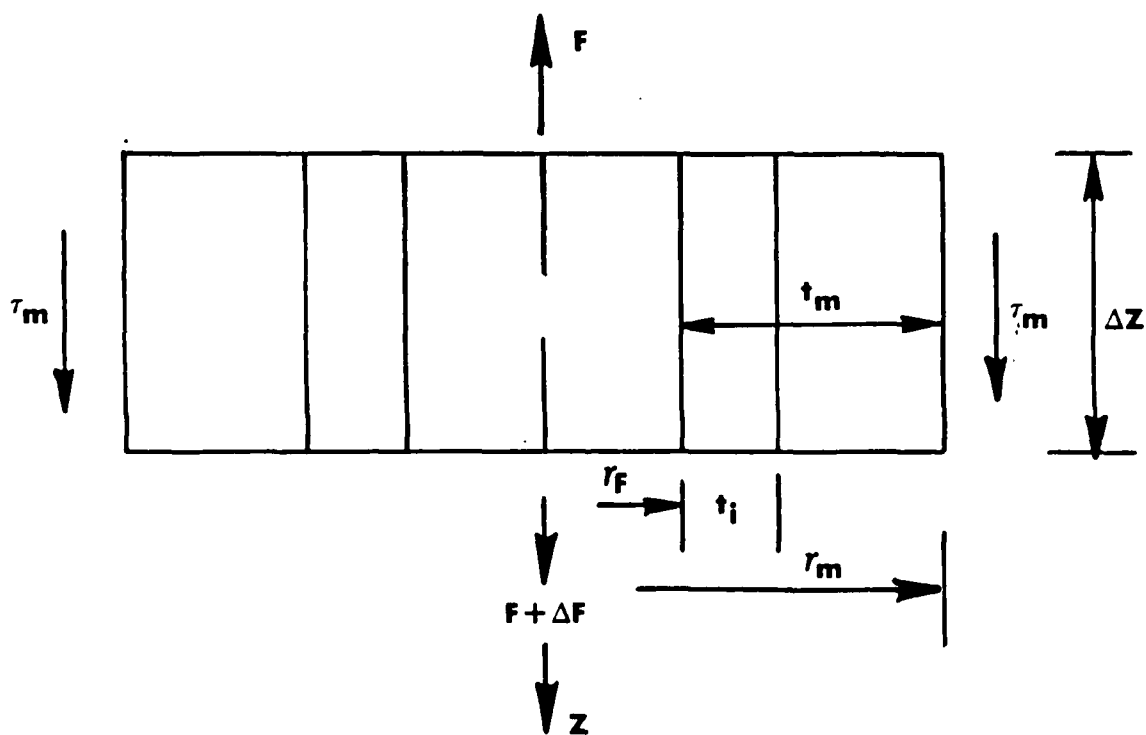
Figure 3b. Free Body Diagram Involving Fiber, Interphase, and Matrix.
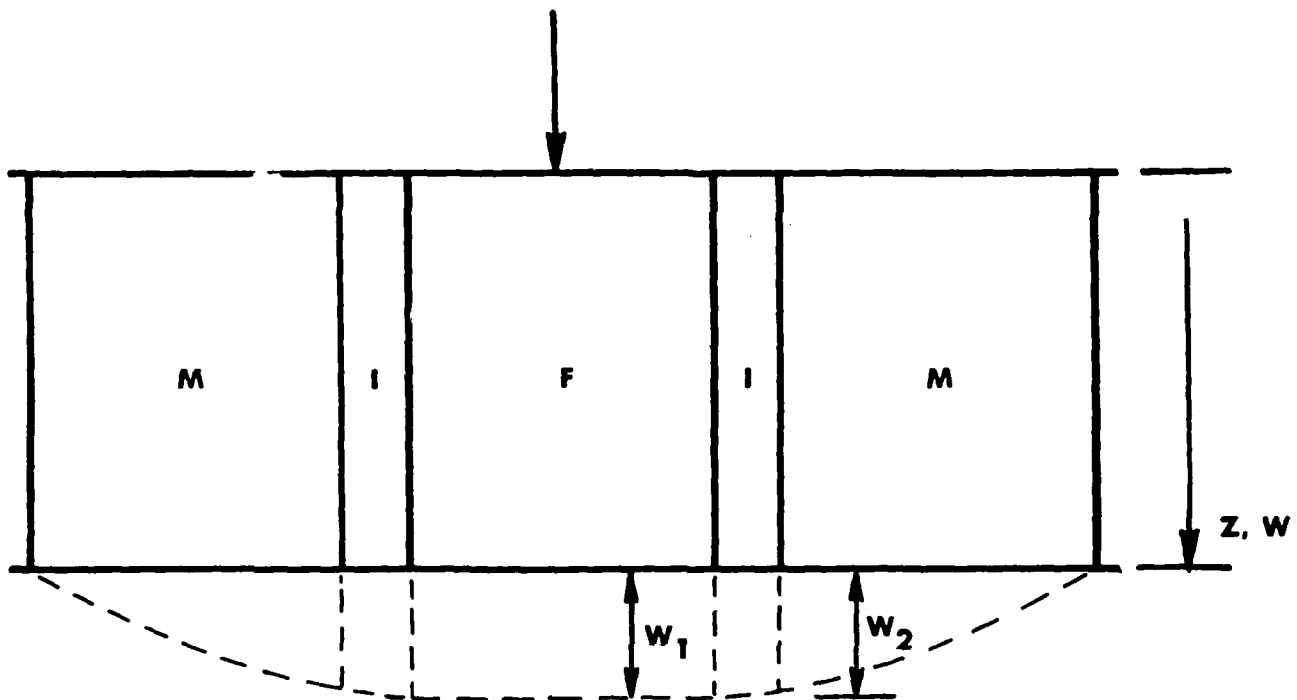
Figure 4. Axial Displacement of Fiber, Interphase, and Matrix.

From equation (3):

$$\tau = \frac{\tau_i r_i}{r} \tag{5}$$

substituting equation (5) into (4) and integrating, we have:

$$w = \frac{\tau_i r_i}{G_i} \ln(r) + C \tag{6}$$

but,

at $\quad r = r_f, \quad w = w_1$

$\quad r = r_i, \quad w = w_2$

Applying these boundary conditions to equation (6), we have:

$$\tau_i = \frac{(w_2 - w_1)G_i}{r_i \ln\left(\dfrac{r_i}{r_f}\right)} \tag{7}$$

By the same procedure and noting that at $r = r_m$, $w = 0$ we have:

$$\tau_m = \frac{-w_2 G_m}{r_m \ln\left(\dfrac{r_m}{r_i}\right)} \tag{8}$$

Also,

$$F = E_f \pi r_f^2 \frac{d\, w_1}{dz} \tag{9}$$

7

substituting equations (7) through (9) into equation (1) and (2) we have:

$$\frac{d^2 w_1}{dz^2} - \frac{2G_i}{E_f r_f^2 \ln\left(\frac{r_i}{r_f}\right)} (w_1 - w_2) = 0 \qquad (10)$$

$$\frac{d^2 w_1}{dz^2} - \frac{2G_m}{r_f^2 E_f \ln\left(\frac{r_m}{r_i}\right)} w_2 = 0 \qquad (11)$$

After some algebraic manipulations of equations (10) and (11), we have:

$$\frac{d^2 w_1}{dz^2} - \alpha^2 w_1 = 0 \qquad (12)$$

where

$$\alpha^2 = \frac{\dfrac{2G_i}{E_f r_f^2 \ln\left(\dfrac{r_i}{r_f}\right)}}{1 + \dfrac{G_i \ln\left(\dfrac{r_m}{r_i}\right)}{G_m \ln\left(\dfrac{r_i}{r_f}\right)}}$$

The solution of equation (12) is:

$$w_1 = C_1 \cosh(\alpha z) + C_2 \sinh(\alpha z) \qquad (13)$$

8

since

$$z = 0, \quad F = -P_0 = -\pi r_f^2 \overline{\sigma} = E_f \pi r_f^2 \frac{dw_1}{dz}$$

$$z = l, \quad w_1 = 0 \tag{14}$$

where $\overline{\sigma}$ is the average applied stress at the fiber end.

Applying the boundary conditions (i.e., equation (14)) to equation (13), we have:

$$w_1 = -\frac{\overline{\sigma}}{E_f \alpha}(-\tanh(\alpha l)\cosh(\alpha z) + \sinh(\alpha z)) \tag{15}$$

w_2 is obtained from equations (11) and (15) such that:

$$w_2 = \frac{r_F^2 E_F \alpha^2 \ln(\frac{r_m}{r_i})}{2G_m} w_1 \tag{16}$$

From equations (7), (15), and (16), the interphase shear stress at $r = r_i$ is written as:

$$\tau_i = \frac{\overline{\sigma}\sqrt{G_m}}{\sqrt{2E_f}} \frac{r_f}{r_i} \frac{(-\tanh(\alpha l)\cosh(\alpha z) + \sinh(\alpha z))}{\sqrt{\frac{G_m}{G_i}\ln(\frac{r_i}{r_f}) + \ln(\frac{r_m}{r_i})}} \tag{17}$$

From equation (3), the interphase shear stress at $r = r_f$ is written as:

$$\overline{\tau_i} = \frac{\overline{\sigma}}{\sqrt{2}}\sqrt{\frac{G_m}{E_f}} \frac{(-\tanh(\alpha l)\cosh(\alpha z) + \sinh(\alpha z))}{\sqrt{\frac{G_m}{G_i}\ln(\frac{r_i}{r_f}) + \ln(\frac{r_m}{r_i})}} \tag{18}$$

The maximum interphase shear stress occurs at:

$$\tau_{max} = (\overline{\tau_i})_{z=0} = -\frac{\overline{\sigma}}{\sqrt{2}}\sqrt{\frac{G_m}{E_f}} \frac{\tanh(\alpha l)}{\sqrt{\frac{G_m}{G_i}\ln(\frac{r_i}{r_f}) + \ln(\frac{r_m}{r_i})}} \tag{19}$$

Note that equation (19) contains two unknowns to be determined (namely, G_i and r_i).

CORRELATION WITH MANDELL'S MICRODEBONDING TESTS

DETERMINATION OF INTERPHASE PROPERTIES

We now postulate that debonding of fiber from the matrix is due to interphase shear failure. Based on this assumption, the debonding criterion for the fiber/matrix interface is written as follows:

$$\tau_0 = \frac{\overline{\sigma_0}}{\sqrt{2}} \sqrt{\frac{G_m}{E_f}} \frac{tanh(\alpha l)}{\sqrt{\frac{G_m}{G_i} ln(\frac{r_i}{r_f}) + ln(\frac{r_m}{r_i})}} \tag{20}$$

where

τ_0 = interphase shear strength

$\overline{\sigma_0}$ = average applied stress at the fiber end which causes fiber-matrix debonding (referred to as the debonding stress).

Let

$$r_i = r_f + t_i$$

$$r_m = r_f + t_m$$

where t_i is interphase thickness and t_m is the thickness combining interphase and matrix.

Equation (20) becomes:

$$\tau_0 = \frac{\overline{\sigma_0}}{\sqrt{2}} \sqrt{\frac{G_m}{E_f}} \frac{tanh(\alpha l)}{\sqrt{(\frac{G_m}{G_i} - 1)ln(1 + \frac{2t_i}{d_f}) + ln(1 + \frac{2t_m}{d_f})}} \tag{21}$$

From equation (21) we conclude that:

$$\frac{\overline{\sigma_0} tanh(\alpha l)}{\sqrt{(\frac{G_m}{G_i} - 1)ln(1 + \frac{2t_i}{d_f}) + ln(1 + 2\frac{t_m}{d_f})}} = constant \tag{22}$$

By selecting $t_m/d_i = 0.4$ and $t_m/d_i = 1.0$ to correlate the test data,[1] the following results were obtained (for detailed calculations, refer to Appendix A).

10

For S-glass/epoxy,

$$(\frac{G_m}{G_i}-1)ln(1+\frac{2t_i}{d_f}) = 1.8446$$

(23)

$$\tau_0 = 39 \, MPa$$

For graphite/epoxy

$$(\frac{G_m}{G_i}-1)ln(1+\frac{2t_i}{d_f}) = 2.0672$$

(24)

$$\tau_0 = 27 \, MPa$$

Note that G_i and t_i cannot be determined separately from equations (23 and (24), but if t_i can be determined from an experiment, then G_i can be determined. Tables 1 and 2 list the interphase properties of S-glass/epoxy and graphite/epoxy, respectively, for various interphase thickness values and show the interphase shear modulus to be softer than bulk matrix for both S-glass/epoxy and graphite/epoxy composite materials.

CORRELATION WITH MICRODEBONDING TEST RESULTS

After the interphase shear strength has been determined, the debonding stress $\bar{\sigma}_0$ is determined as follows:

$$\overline{\sigma_0} = \sqrt{2}\tau_0\sqrt{\frac{E_f}{G_m}}\sqrt{(\frac{G_m}{G_i}-1)ln(1+\frac{2t_i}{d_f})+ln(1+\frac{2t_m}{d_f})}$$

(25)

Making use of equations (23) and (24), and noted that we have for S-glass/epoxy:

$$\overline{\sigma_0} = \tau_0\sqrt{2\frac{E_f}{G_m}}\sqrt{1.8446+ln(1+\frac{2t_m}{d_f})}$$

(26)

and for graphite/epoxy:

$$\overline{\sigma_0} = \tau_0\sqrt{2\frac{E_f}{G_m}}\sqrt{(2.0672+ln(1+\frac{2t_m}{d_f})}$$

(27)

Equations (26) and (27) are plotted in Figures 5 and 6. The correlations with the microdebonding test results are excellent.

Table 1. Interphase Properties of S-glass Epoxy

Interphase Shear Strength = 39 MPA

t_i/d_f	t_i (nm)	G_m/G_i
.001	10	922
.005	50	184
.01	100	92
.05	500	18
.1	1000	9.0

Table 2. Interphase Properties of Graphite/Epoxy

Interphase Shear Strength = 27 MPA

t_i/d_f	t_i (nm)	G_m/G_i
.0014	10	724
.0071	50	145
.0143	100	74
.0714	500	15
.143	1000	7
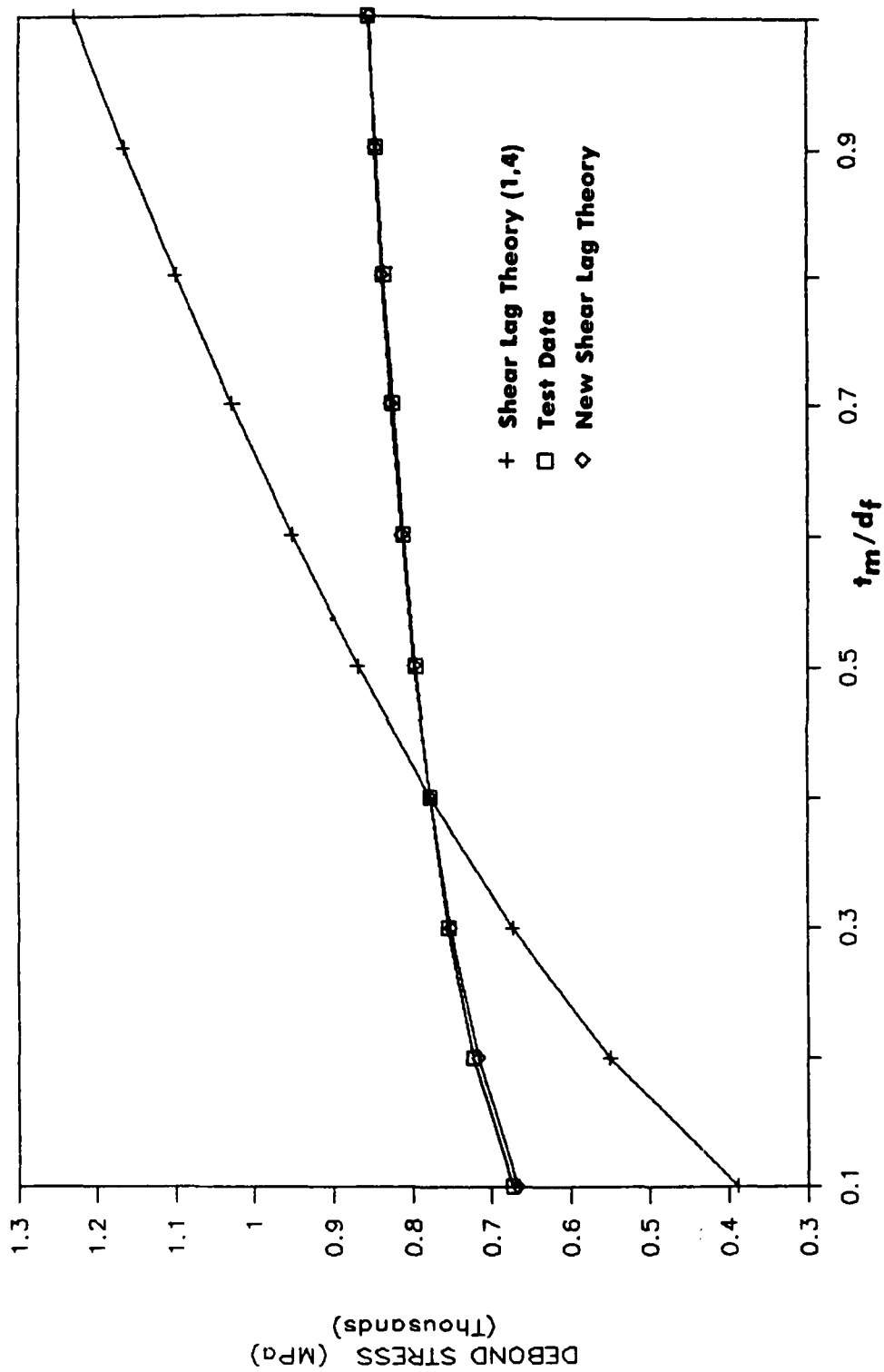
Figure 5. Variation of Debond Stress vs. t_m/d_f for S-glass/Epoxy.
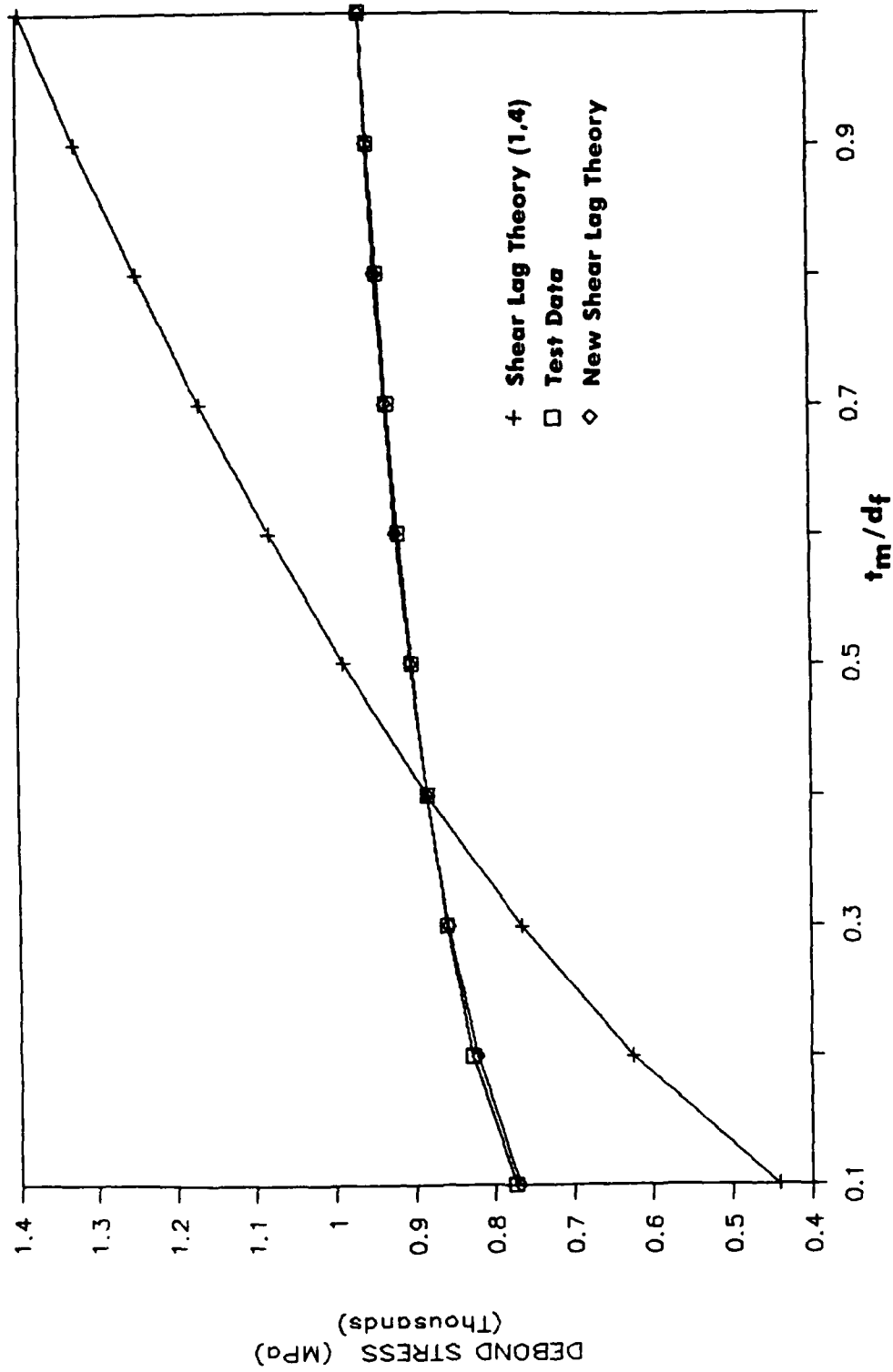
Figure 6. Variation of Debond Stress vs. t_m/d_f for Graphite/Epoxy.

INFLUENCE OF INTERPHASE PROPERTIES ON INTERPHASE
SHEAR AND FRACTURE TOUGHNESS OF COMPOSITES

INTERPHASE SHEAR STRESS

Equation (19) can be rewritten as:

$$\frac{\tau_{max}}{\sigma} = \frac{-1}{\sqrt{2}}\sqrt{\frac{G_m}{E_f}}\frac{1}{\sqrt{(\frac{G_m}{G_i}-1)ln(1+\frac{2t_i}{d_f})+ln(1+\frac{2t_m}{d_f})}} \tag{28}$$

Let

$$K_s = (\text{stress concentration factor}) = \frac{|\tau_{max}|}{\sigma}\sqrt{\frac{E_f}{G_m}} \tag{29}$$

Thus

$$K_s = \frac{1}{\sqrt{2}}\frac{1}{\sqrt{(\frac{G_m}{G_i}-1)ln(1+\frac{2t_i}{d_f})+ln(1+\frac{2t_m}{d_f})}} \tag{30}$$

Equation (30) is plotted in Figures 7 and 8 for K_s vs. G_m/G_i for various ratios. We can conclude that:

(1) The lower the G_m/G_i ratio, the higher the stress concentration and the more likely debonding.

(2) The thinner the interphase thickness, t_i, the higher the stress concentration, again making debonding easier.

MODE I FRACTURE TOUGHNESS

Murphy,[3] etc., showed that the Mode I fracture energy of unidirectional composites can be expressed as follows:

$$(G_I)_c \approx (1-v_f)G_M + v_f(G_F + G_{INF}) \tag{31}$$

where

$(G_I)_c$ = Mode I fracture energy of composite
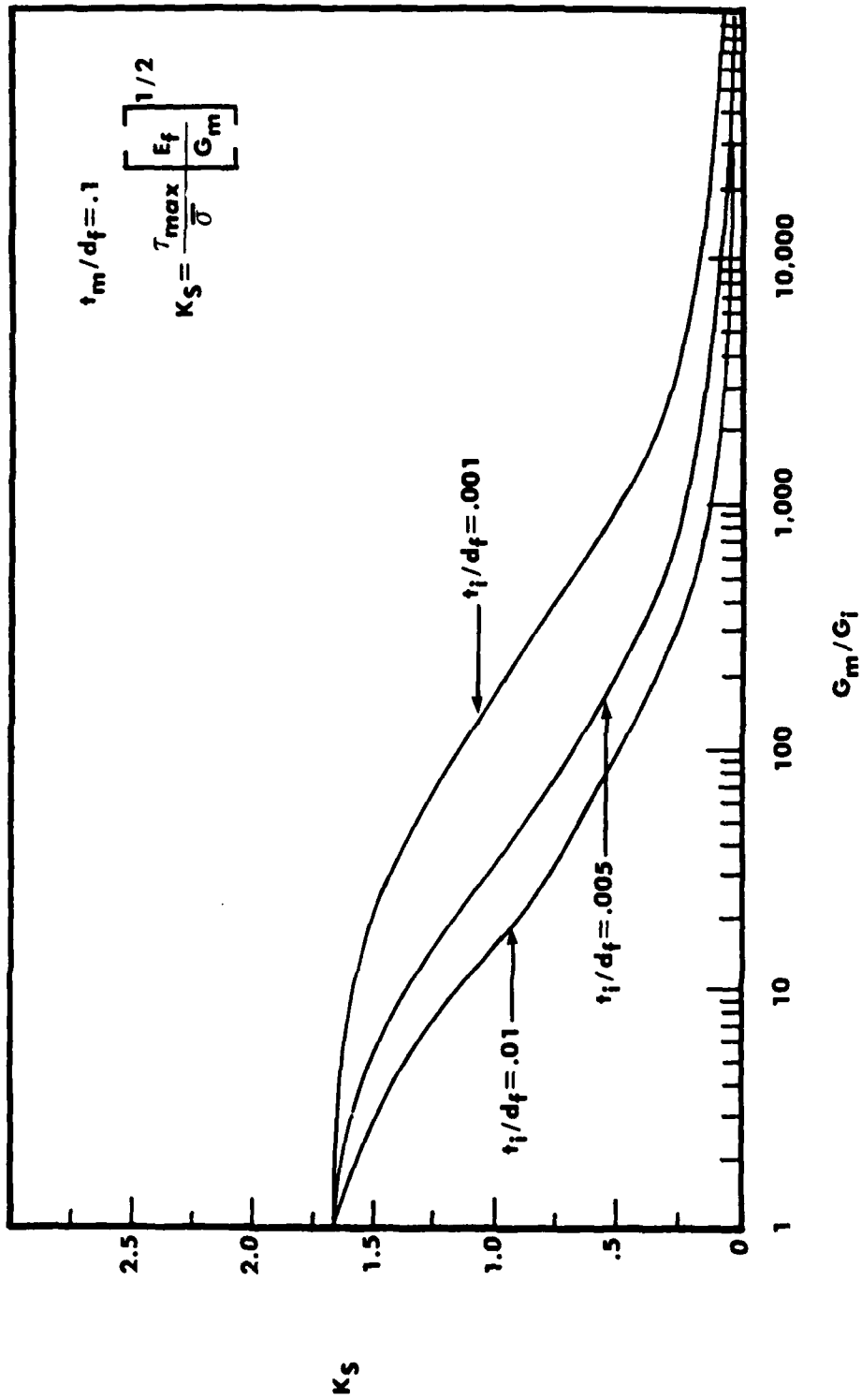
Figure 7. Effect of Interphase Shear Modulus on Maximum Stress for $t_m/d_f = 0.1$.
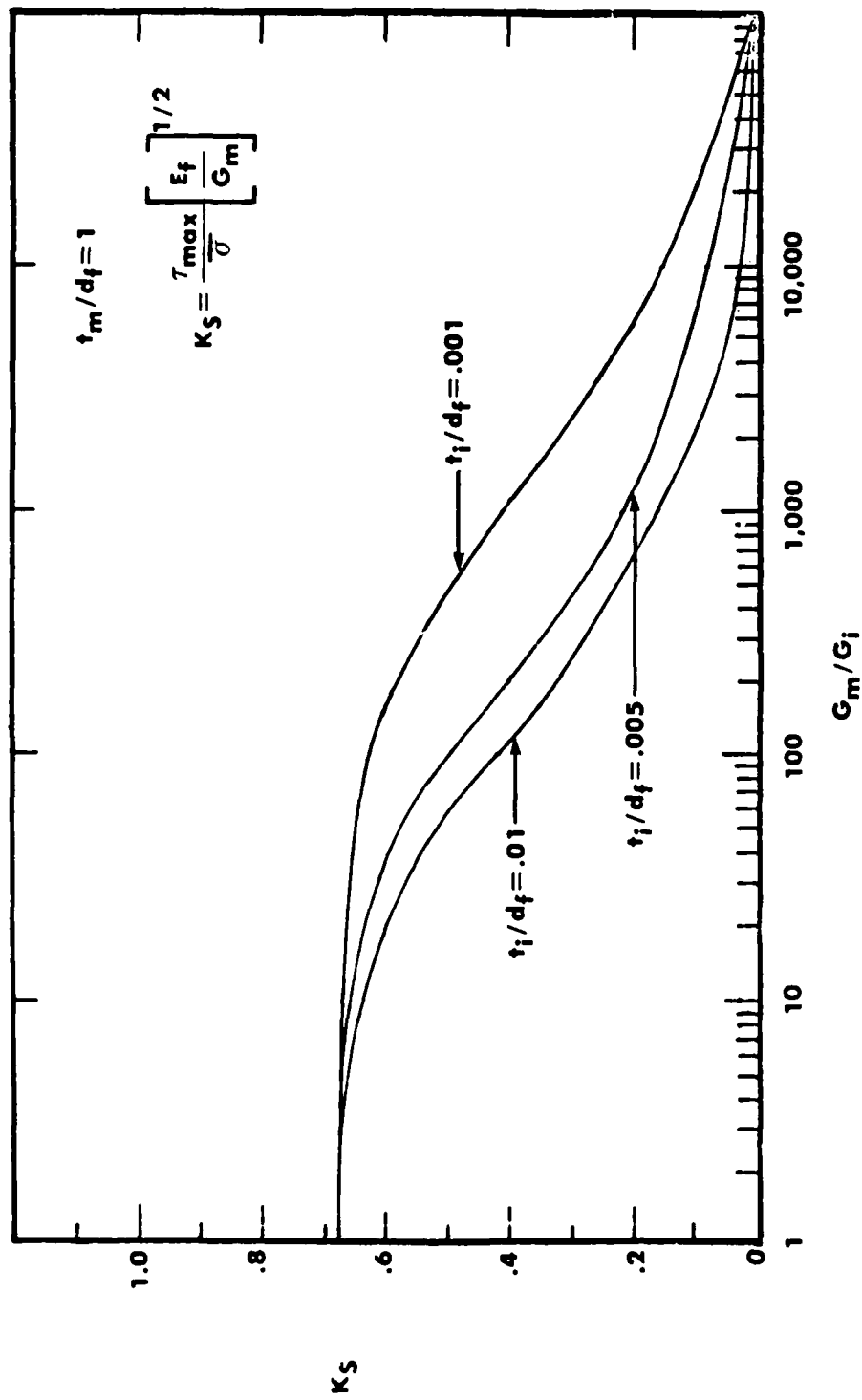
Figure 8. Effect of Interphase Shear Modulus on Maximum Interfacial Shear Stress for $t_m/d_f = 1.0$.

G_M = Mode I fracture energy of matrix

G_F = Mode I fracture energy of fiber

v_f = volume fraction of fiber

G_{INF} = Mode I fracture energy associated with the decohesion of the fiber matrix interface.

Murphy further showed that:

$$G_{INF} = \frac{d_f \sigma_{fu}^3}{4\tau_f E_f} (1 - g + g^2 - g^3 + \frac{1}{2}(\frac{l_p}{l_d})^2 (\frac{E_f}{\sigma_{fu}})(1-g)^2)$$

(32)

where

σ_{fu} = ultimate stress of fiber

l_d = $(d_f/4\tau_f)(\sigma_{fu} - \bar{\sigma}_0)$

$\bar{\sigma}_0$ = debonding stress

l_p = fiber pull-out length

τ_f = post debonding friction shear stress

$$g = \frac{\bar{\sigma}_0}{\sigma_{fu}}$$ = debonding fracture ratio

(33)

Examining equations (31) and (32), it can be seen that the smaller the g (i.e., weaker interface), the larger the G_{INF} and hence, the tougher the composite. On the other hand, the larger, the g (i.e., stronger interface), the smaller the G_{INF} yielding a more brittle composite. If g = 1, (i.e., the fiber breaks with no debonding between fiber and matrix), equation (31) reduces to:

$$(G_I)_c = (1-v_f) G_M + v_f G_F$$

Murphy[3] showed that for high-volume fractions the Mode I fracture energy, $(G_I)_c$, of composites can range over five orders of magnitude, while the debonding fracture ratio, g, ranges from zero to one.

From equations (29) and (33), g can be expressed as follows:

$$g = \frac{\tau_0}{\sigma_{fu}} \frac{1}{K_s} \sqrt{\frac{E_f}{G_m}}$$

(34)

18

To demonstrate how interphase properties will effect the Mode I fracture toughness of the composite, equation (32) is rewritten as follows:

$$\frac{G_{INF}}{C_{INF}} = 1-g+g^2-g^3+\frac{1}{2}(\frac{l_p}{l_d})^2(1-g)^2 \tag{35}$$

where

$$C_{INF} = \frac{d_f\sigma_{fu}^3}{4\tau_f E_f}$$

For simplicity, assume $l_p=0$ (i.e., no fiber pull-out occurs during fracture of composite). Equation (35) then becomes:

$$\frac{G_{INF}}{C_{INF}} = 1-g+g^2-g^3 \tag{36}$$

Assuming that the interphase strength, τ_0, is constant for various interphase thicknesses and making use of equation (34), equation (36) is plotted as shown in Figures 9 and 10. The detailed calculation is shown in Appendix B.

From the plots, it can be seen that when the interphase property, G_i, is closer to the bulk matrix, G_m, the composite material will have higher fracture toughness. Note that the thinner the interphase thickness, t_i, the tougher the composite material.

FINITE ELEMENT SIMULATION

MICRODEBONDING PROBLEM

An axisymmetric finite element model that includes the interphase was developed. Interphase properties were obtained by either using the values contained in Tables 1 and 2 or those derived from using equation (23) for S-glass/epoxy and equation (24) for graphite/epoxy for various interphase thicknesses. Only those results for graphite/epoxy are presented. Figures 11 and 12 are typical models used to analyze the microdebonding problem. The NASTRAN computer code was used to perform the analysis. Note that the top surface and side surface corresponding to outside radius were assumed fixed. A 1 N force was applied at the center of the cylindrical composite disc.

Figure 13 shows the typical interphase shear distribution along the axis. The maximum shear stress occurs at approximately 0.4 fiber diameter below the surface. Shear lag theory positions the maximum shear at the surface. Note that the magnitude of the interface shear for composite without an interphase (i.e., $G_m/G_i=1.0$) is much higher than for a composite with an interphase. This result agrees with the conclusion from the shear lag analysis in the foregoing section.
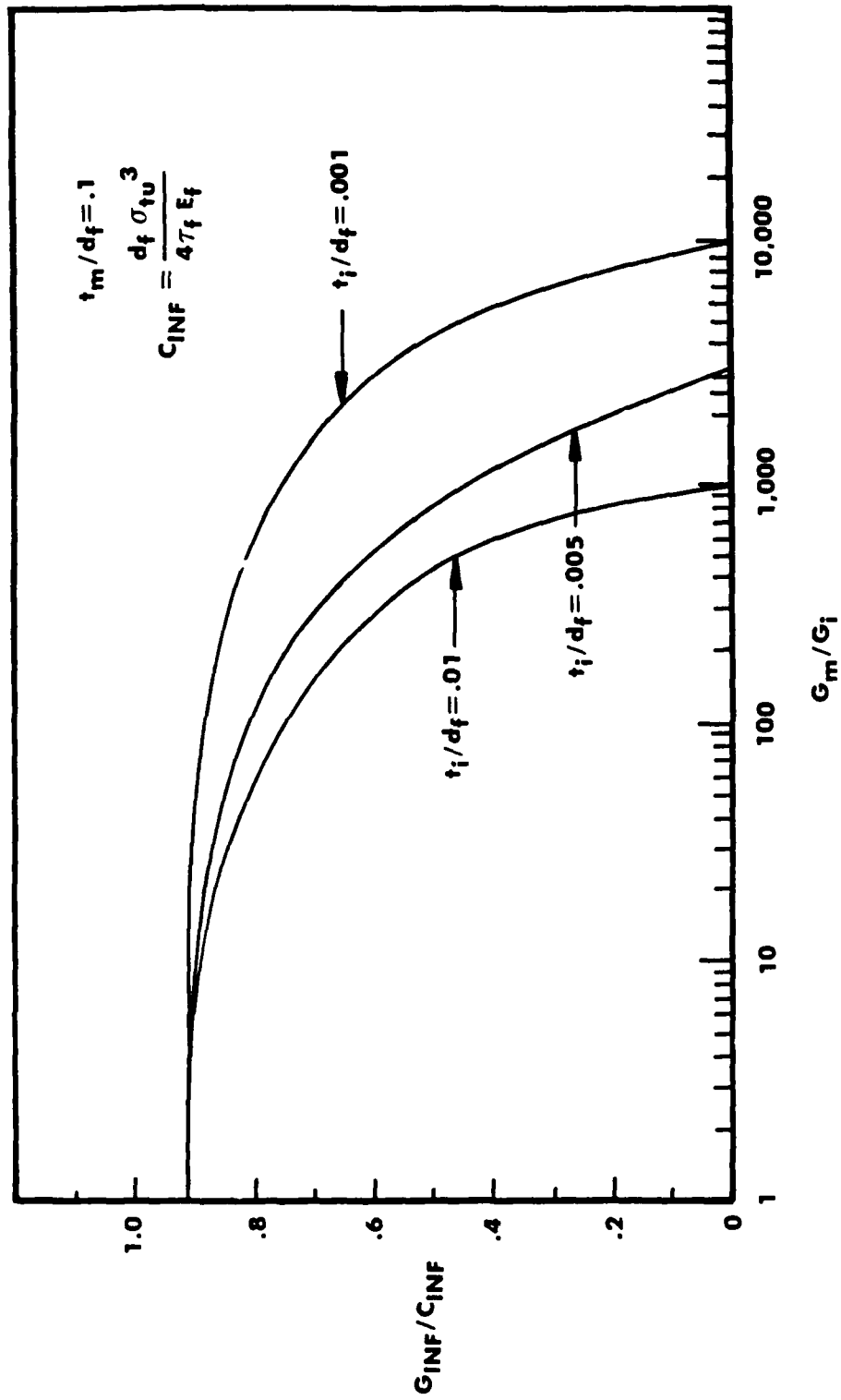
Figure 9. Effect of Interphase on Opening Mode Fracture Energy of a Unidirectional Fiber Composite for $t_m/d_f = 0.1$.

20
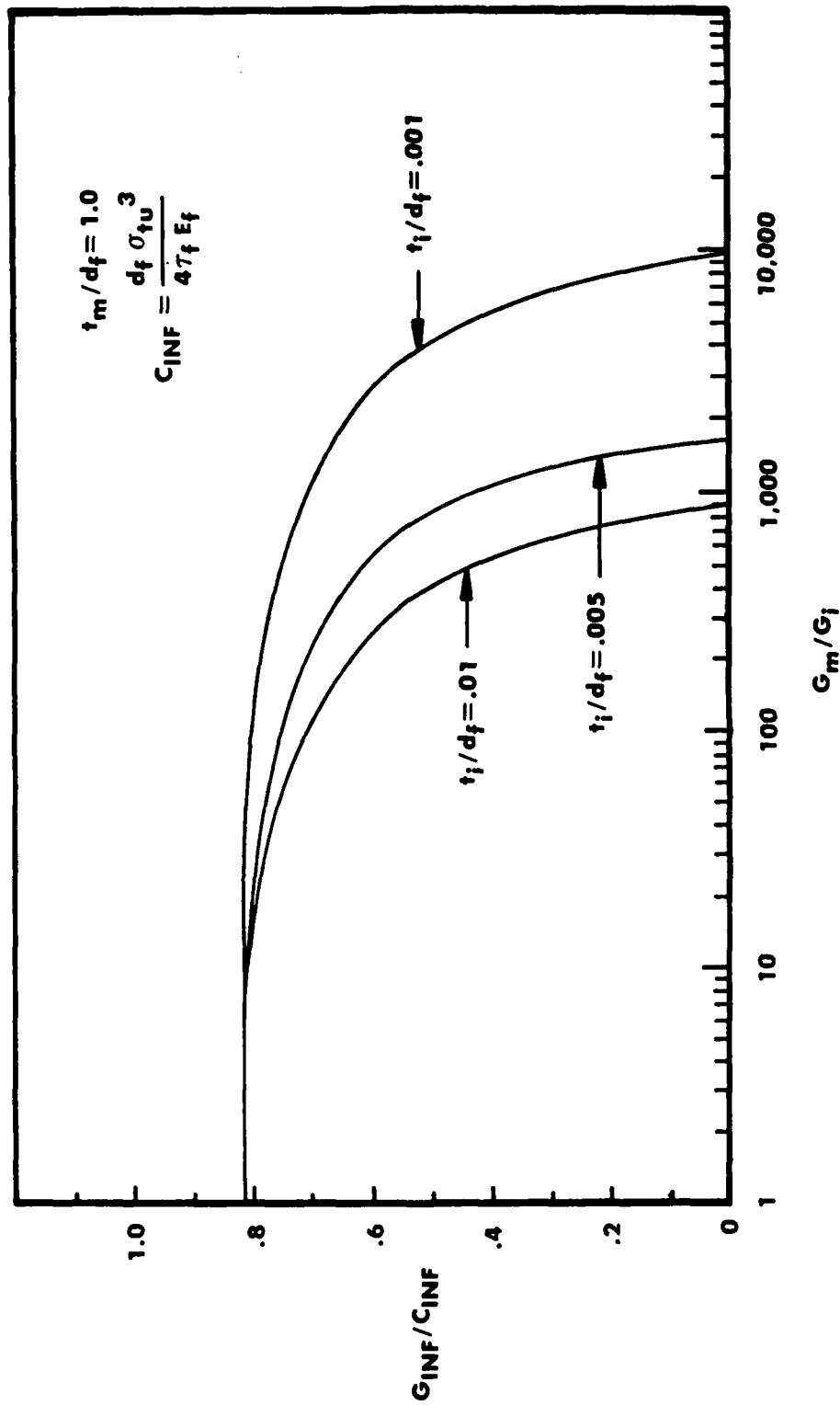
Figure 10. Effect of Interphase on Opening Mode Fracture Energy
of a Unidirectional Fiber Composite for $t_m/d_f = 1.0$
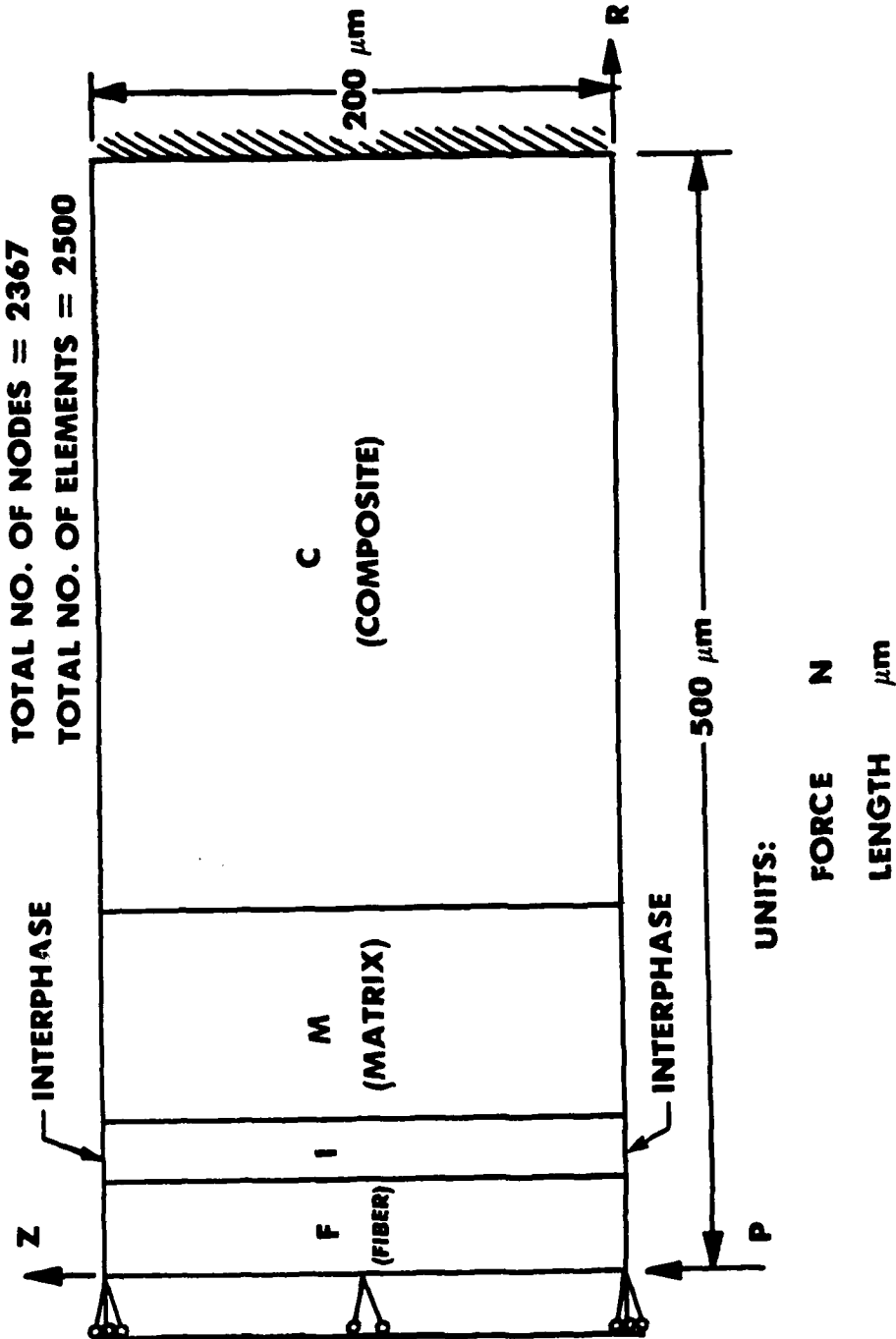
Figure 11. Finite Element Model for Axisymmetric Solid.

TOTAL NO. OF NODES = 2367
TOTAL NO. OF ELEMENTS = 2500

200 μm

R

C
(COMPOSITE)

INTERPHASE

M
(MATRIX)

INTERPHASE

I

F
(FIBER)

Z

P

500 μm

UNITS:

FORCE   N

LENGTH   μm

Figure 12. Axisymmetric Finite Element Model for Microdebonding Problem.
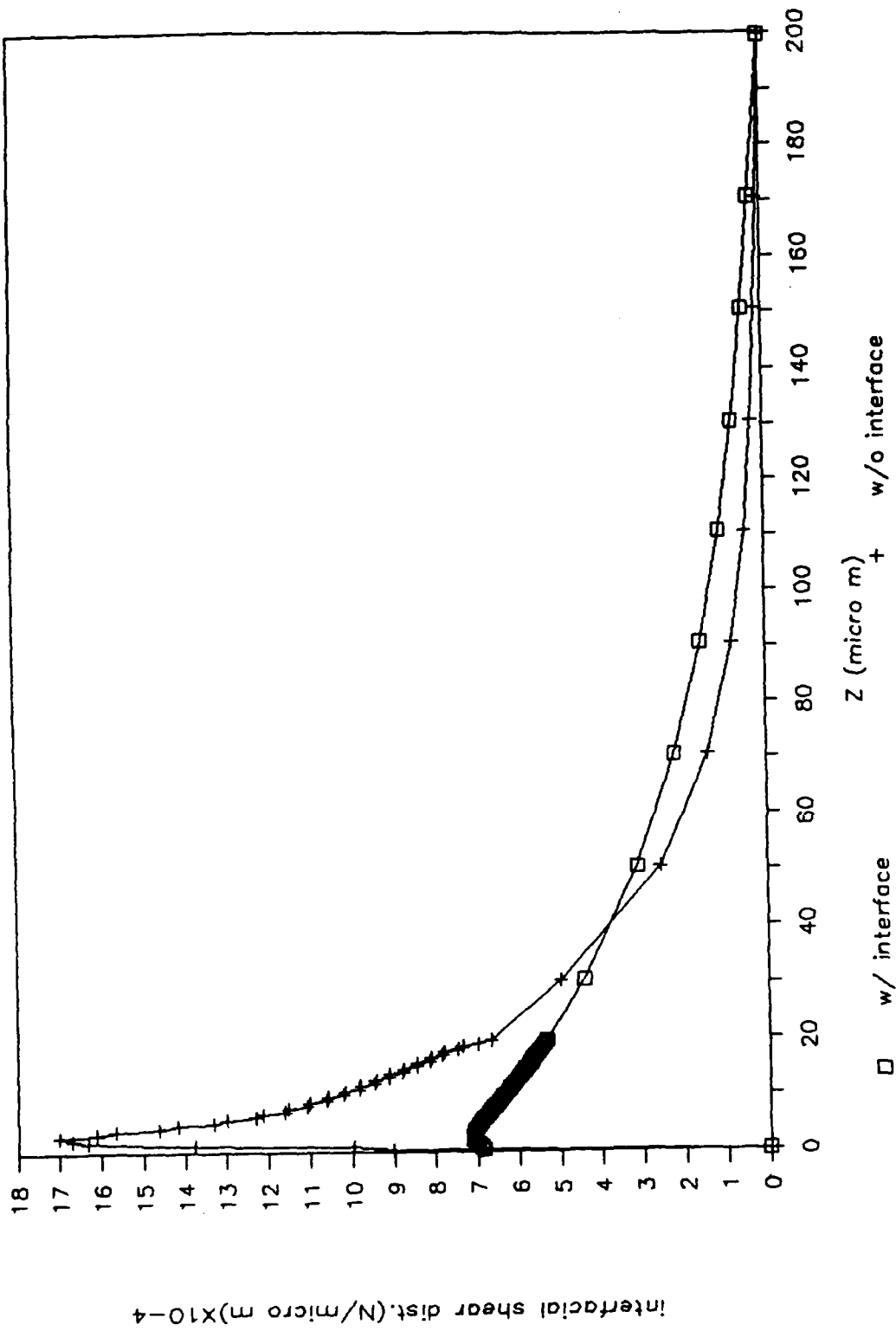
Figure 13. Interphase Effect on Interfacial Shear ($t_m/d_f=0.36$, $V_f=0.4$, $t_i=0.1$ µm).

$\square$ w/ interface $+$ w/o interface

Z (micro m)

interfacial shear dist.(N/micro m)x10-4

Figure 14 shows the prediction of debonding stress $\bar{\sigma}_0$, for $t_m/d_f = 0.1$ and $t_m/d_f = 1.0$, where data for $t_m/d_f = 0.4$ was used to determine the interphase shear strength. We see that the model, which includes the interphase, provides a better solution than those without the interphase.

Also, note that interphase shear strength predicted by finite element analysis, 23.9 mpa, is close to that predicted by the shear lag theory. (For detailed calculation, refer to Appendix A. This interphase shear strength value is different from the values of interfacial shear strength obtained by other investigators.[1]

Figure 15 shows the fiber end displacement in the axial direction under a 1.0 N axial load applied at the fiber end. The correlation between the finite element analysis and new shear lag theory is very good, validating the adequacy of the shear lag theory.

INTERPHASE EFFECT ON OUT-OF-PLANE DISPLACEMENT

Finite element calculations were performed to determine the effect of the interphase on the out-of-plane displacement using the model shown in Figure 16. This model corresponds to the experimental geometry used for tensioned fiber tests in reference 14. Figures 17 and 18 show the predicted out-of-plane displacements with and without interphase for $G_m/G_i = 25$ and $G_m/G_i = 74$ respectively. It can be seen that a significant displacement gradient occurs in the vicinity of interphase region. Thus, the interphase region may be defined as a region with a very high displacement gradient allowing the dimension of interphase to be determined through direct measurement of the length of this high displacement gradient region.

The results shown in Figures 17 and 18 were adjusted for a 0.4% fiber strain load and correlated with test results[15] as shown in Figure 19. Interphase properties with $G_m/G_i = 25$ and $t_i = 0.1\mu m$ match the test data. However, if this method is not believed adequate to determine the exact interphase thickness, then the radial displacement field must also be measured in addition to the axial displacement field so that the test results can be correlated to determine separate values for the interphase thickness and modulus. Note that the softer the interphase, the greater the displacement gradient in the interphase region.

DISCUSSION AND CONCLUSION
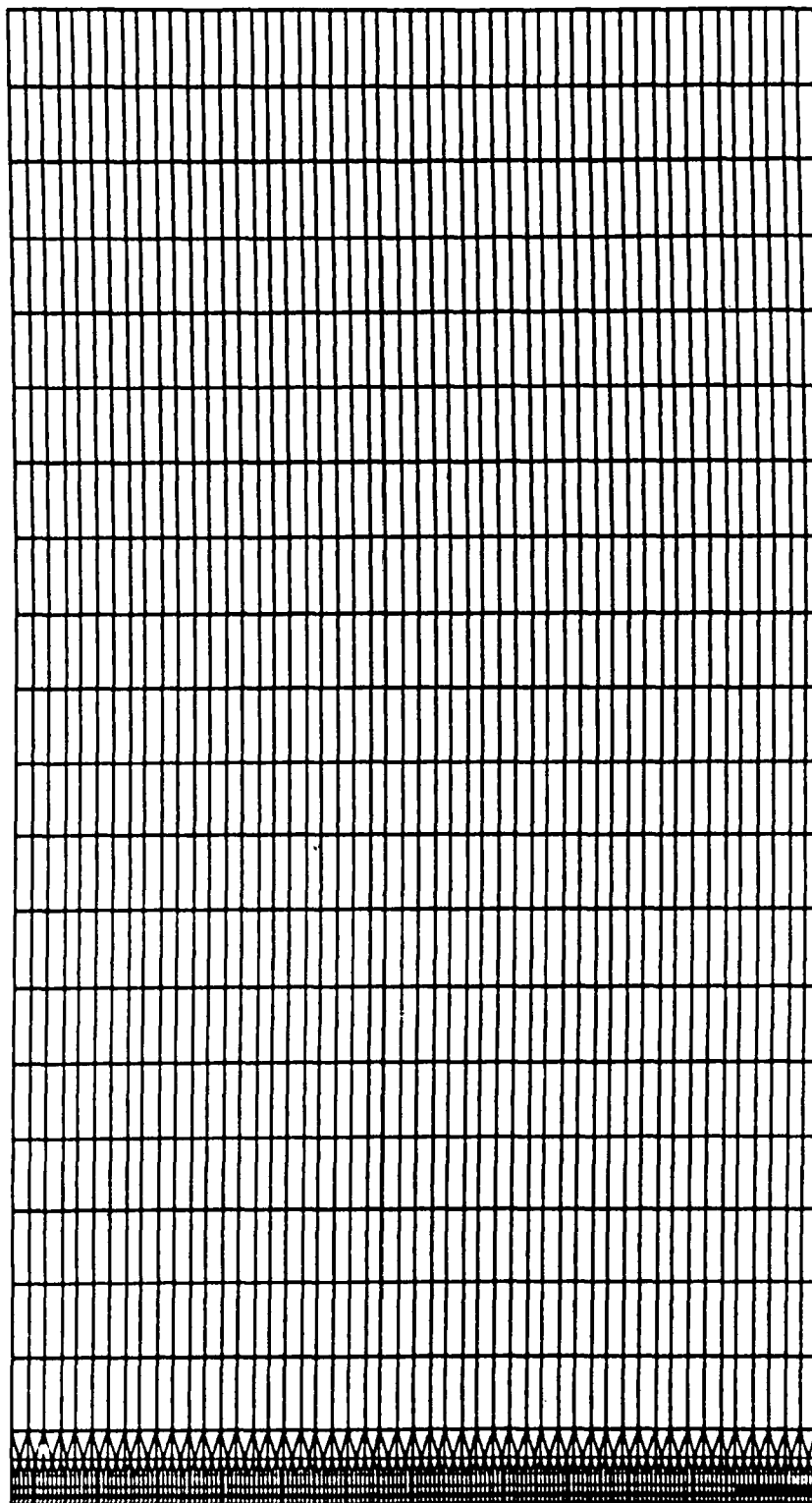
The ratio between interphase shear modulus and thickness can be established from shear lag analysis, but not specific values for G_i or T_i separately. If the interphase thickness can be determined from an experimental measurement, then equation (23) or equation (24) can be used to calculate the interphase shear modulus for S-glass/epoxy and graphite/epoxy, respectively. If the interphase thickness is not available experimentally, then an iteration procedure must be performed using equations (23) and (24) as starting values for interphase shear modulus and thickness. Iterate G_i and T_i until the analytical results (i.e., out-of-plane displacement and radial displacement) converge to the test results. More studies need to be pursued of this approach to compute G_i or T_i.

In this report it is assumed that the interphase is an axisymmetric region of uniform modulus and fixed radial dimension. We recognize that the true interphase region has radially varying properties and can also exhibit circumferential property gradients.

For a tougher composite, equation (32) and Figures 9 and 10 suggest that the composite material must possess:

1. Larger fiber diameter and fiber ultimate stress

2. Smaller post debond frictional shear stress and fiber Young's modulus

3. Smaller interphase shear strength

4. Smaller interphase thickness and G_m/G_i ratio.

Although interphase shear strength, τ_0, and post debond frictional shear stress vary with interphase thickness, t_i, Figures 9 and 10 give approximate guidelines for obtaining tougher composite materials. Note that the weaker interface (i.e., small interphase shear strength) provides tougher fracture resistance, but may affect the strength of composite, especially short fiber composites.

The following conclusions are drawn from this study:

1. By including the interphase, both shear lag analysis and finite element analysis provide much better predictions of material response.

2. The interphase exists and is softer than the matrix for the composites used by Mandell in his microdebonding tests (i.e., S-glass/epoxy and graphite/epoxy).

3. The properties and thickness of the interphase have significant influence on the interface stress, displacement, and fracture toughness of fibrous composites.
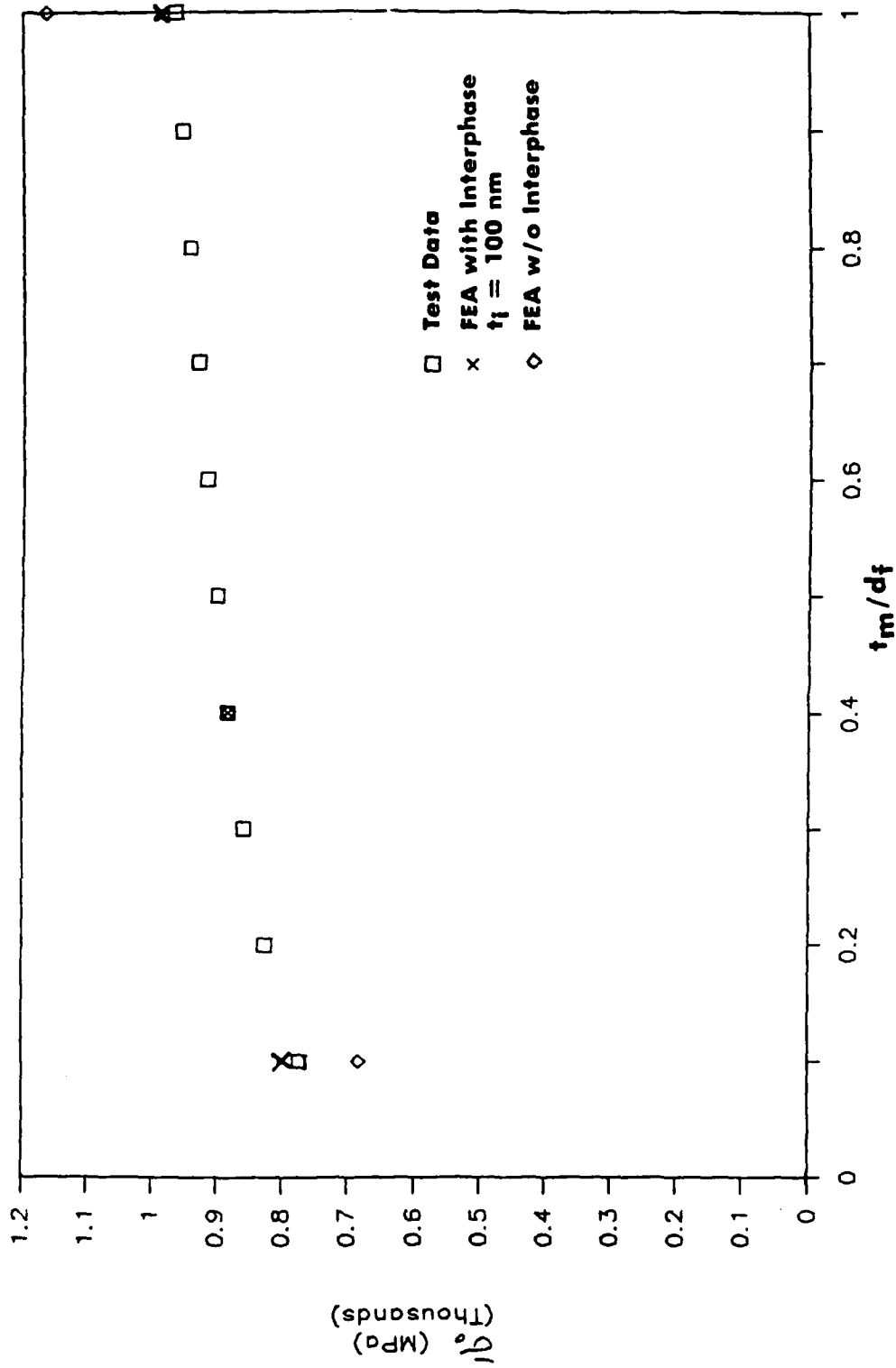
Figure 14. Variation of σ_0 vs. t_m/d_f as Predicted by FFEA With and Without Interphase for Graphite/Epoxy.
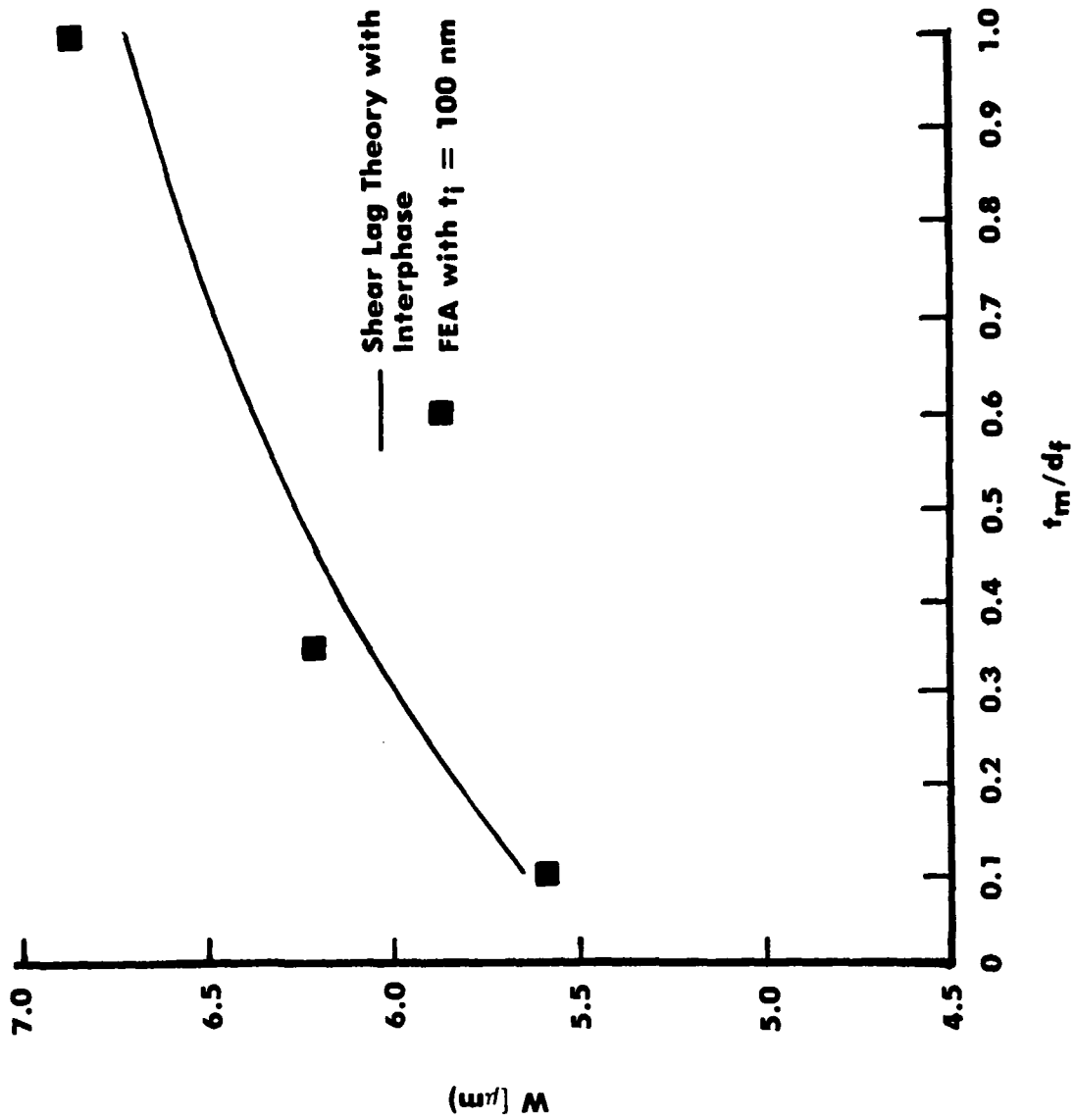
Figure 15. Axial Displacement of Fiber End Under 1 N Load Applied at Fiber End.
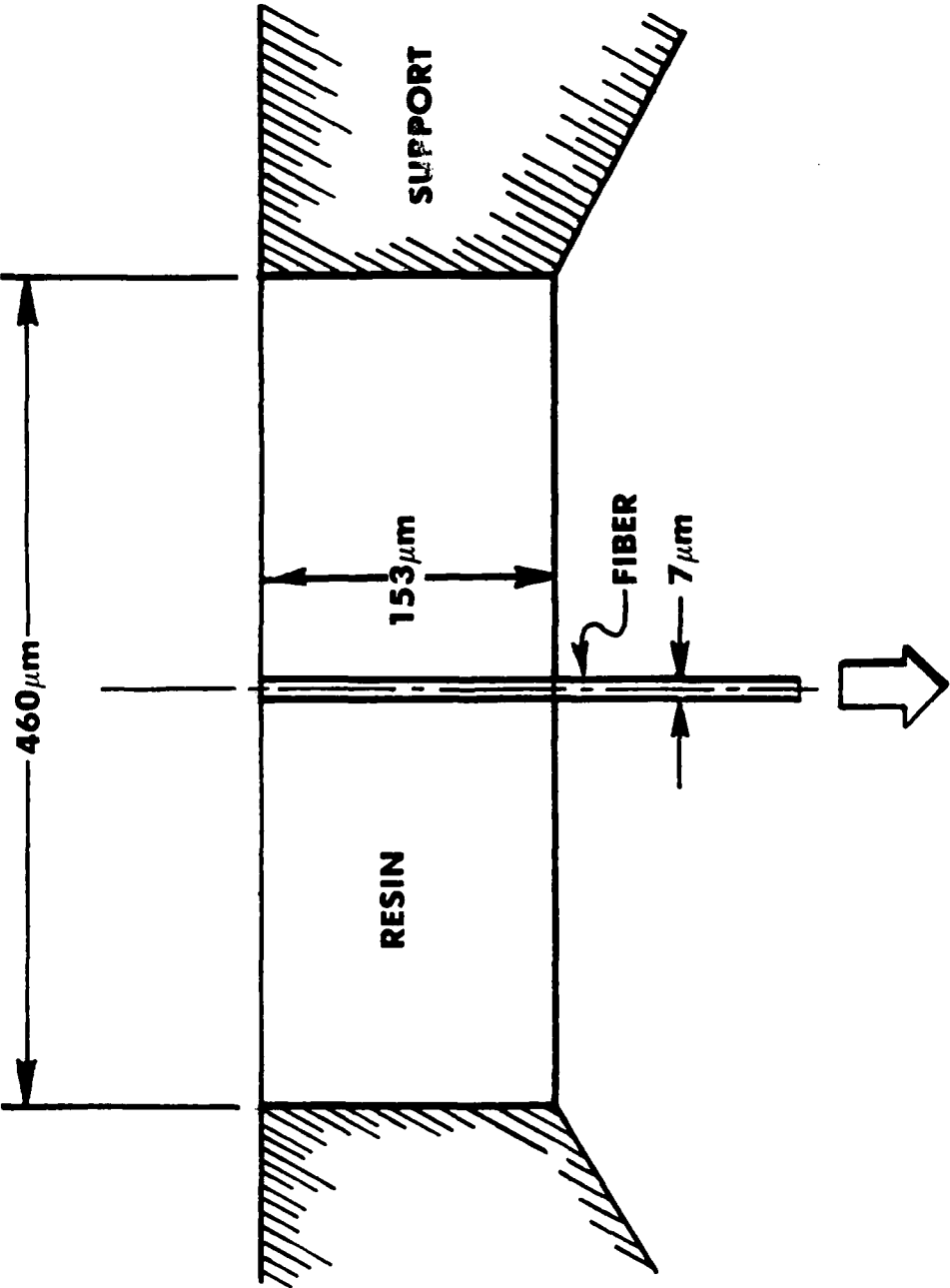
Figure 16. Modeling of Matrix Deformation Near Loaded Fiber.
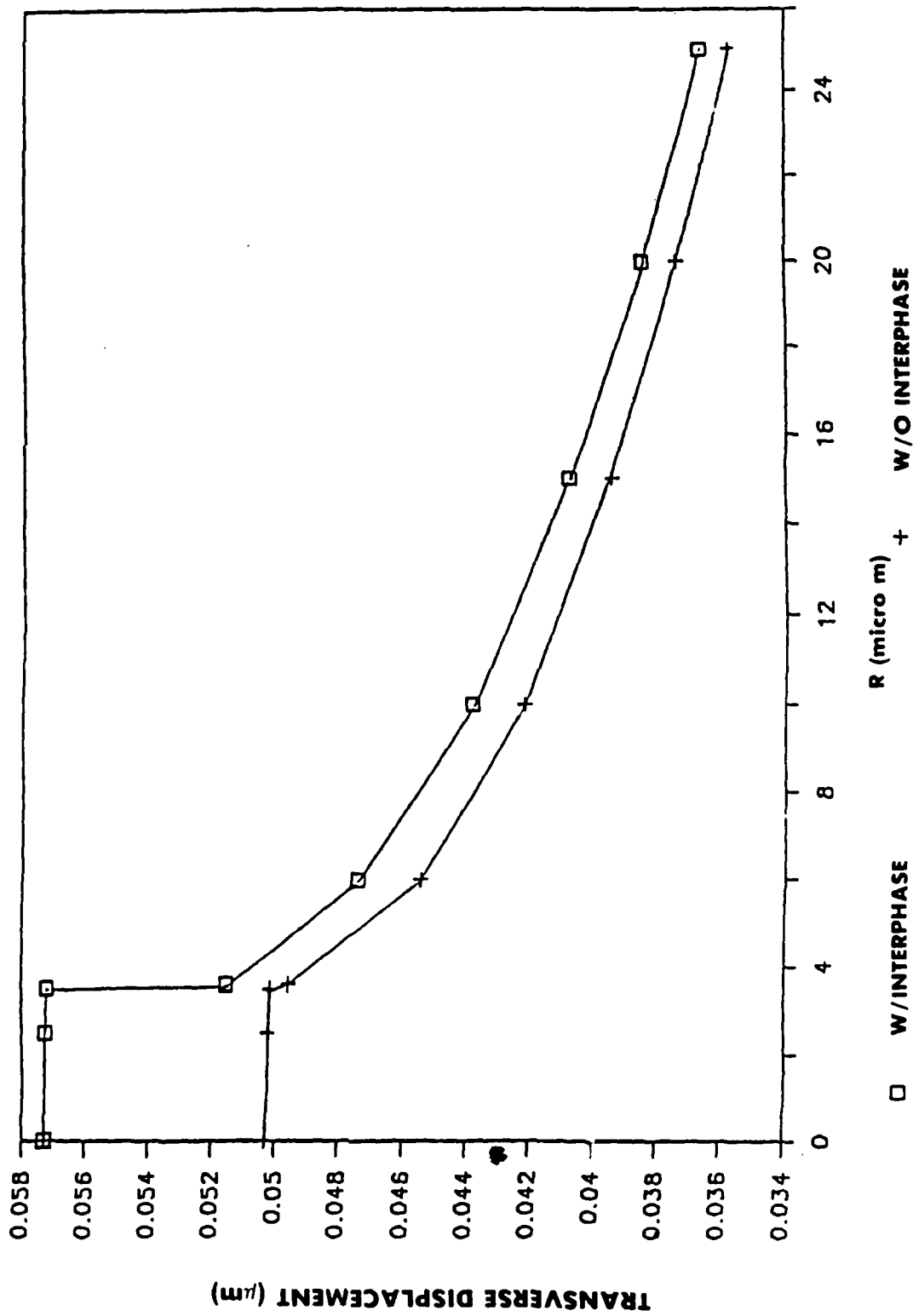
Figure 17. Interphase Effect on Displacement at Top Surface
(P=0.017N, t_i=0.1 μm), G_m/G_i=25).
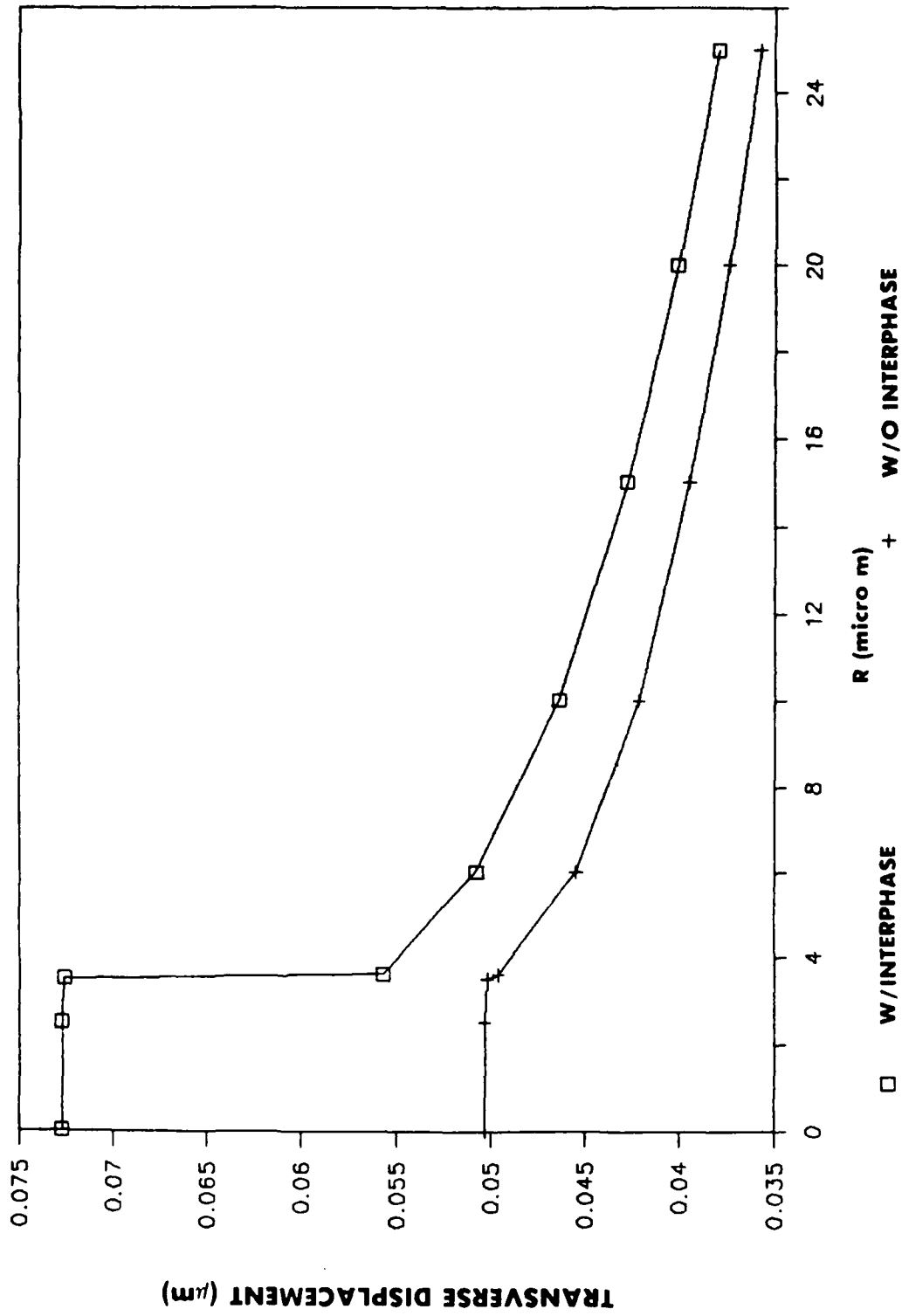
Figure 18. Interphase Effect on Displacement at Top Surface
$(P = -0.017N, t_i = 0.1\ \mu m)$, $G_m/G_i = 74)$.
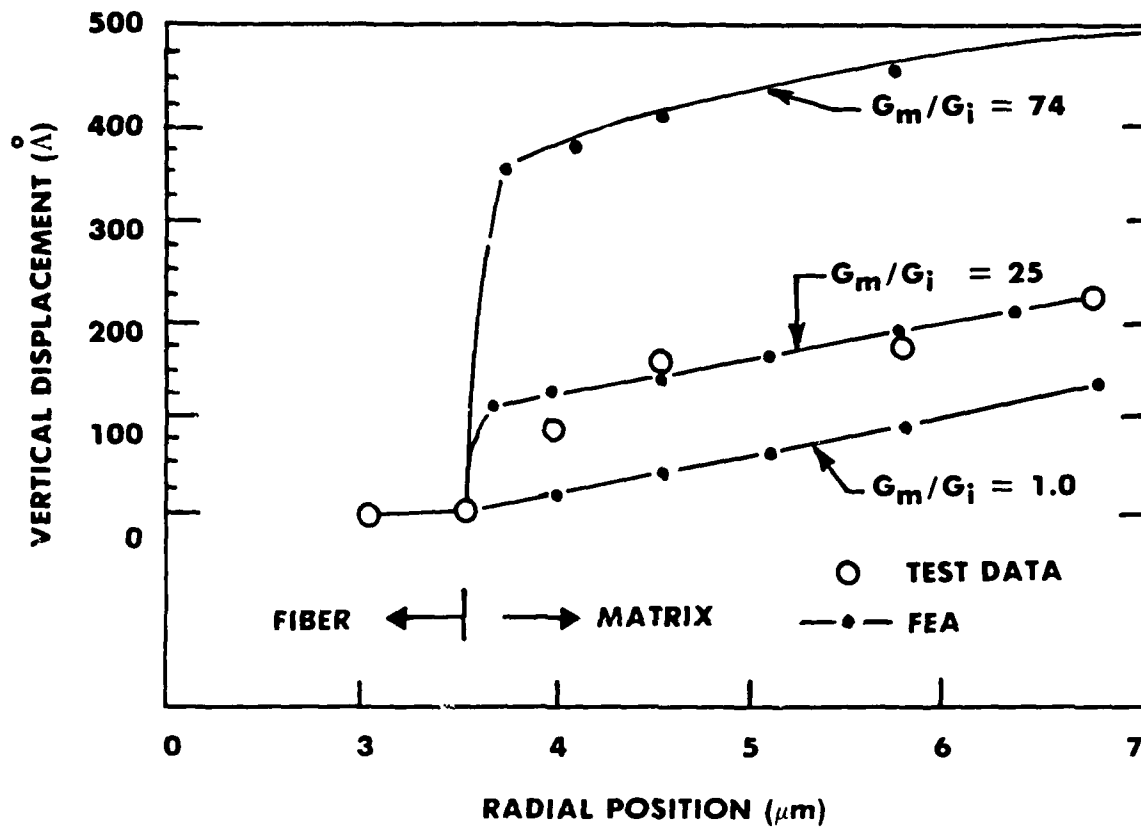
Figure 19. Correlation of Finite Element Analysis and Out-of-Plane Displacement Test Data for 0.4% Fiber Strain Load With $t_i = 0.1\mu$ m.

REFERENCES

1. Mandell, J.F., et al. "Modified Micro-debonding Test for Direct *In-Situ* Fiber/Matrix Bond Strength Determination in Fiber Composites," Composite Materials (Seventh Conference). ASTM STP 893.

2. Chamis, C.C. "Mechanics of Load Transfer at the Fiber/Matrix Interface," NASA TN D-6588, February 1972.

3. Murphy, M.C. and Outwater, J.O. "The Toughness of Reinforced Plastics," 28th Annual Technical Conference 1973. Reinforced Plastic/Composites Institute. The Society of Plastics Industry, Inc.

4. Greszczuk, L.B. "Theoretical Studies of the Mechanics of the Fiber-Matrix Interface in Composites," ASTM STP 452, American Society for Testing and Materials, Philadelphia, p. 42, 1969.

5. Cox, H.L. Br. J. Appl. Phys. 16, p. 199 (1952).

6. Piggott, M.R. "Load Bearing Fibre Composites" Pergamon, Oxford (1980).

7. Remedios, N.C. and Wood, W.G. "Stress Transfer from a Loaded Matrix to a Single Fiber," J. Composite Material, Vol. 2, 1968, pp. 517-520.

8. Carraron, A.S. and McGarry, F.J. "Matrix and Interface Stresses in a Discontinuous Fiber Composite Model," J. Composite Mat. Vol 2, No. 2, April 1968, p. 222.

9. Harner, Juan, Ashbaugh, Noel, et al. "Investigation of Micromechanical Behavior of Fiber Reinforced Plastics," Wittaker Corp. (USAAVLABS-TR-67-66, AD-667901), February 1968.

10. Drzal, Lawrence T. "Tough Composite Materials: Recent Developments," Published by Noyes Pub., Park Ridge, NJ, 1985, pp. 207-222.

11. Piggott, M.R. Polymer Composites *8* (5), 1987, pp 291-296.

12. Garton, Andrew; Daly; John H. Polymer Composites *6* (4), 1985.

13. Shelton, C.G. and Marks, P.R. Journal of Material Science Letters *7* (6) 1988, pp. 673-675.

14. Williams, J.G., Donnellan, M.E., et al. "Properties of the Interphase in Organic Matrix Composites," Journal of Material Science, January 1990.

15. James, M.R., Morris, W.L., and Dadkhah, M. "Determination of Interfacial Properties," Interim report for period 1 March through 15 June 1989. Contract No. N00014-89-C-0083, Rockwell International Science Center, June 1989.

THIS PAGE INTENTIONALLY LEFT BLANK

APPENDIX A: DETERMINATION OF INTERPHASE PROPERTIES
FOR S-GLASS/EPOXY AND GRAPHITE/EPOXY

NEW SHEAR LAG THEORY

INTERPHASE PROPERTIES

From equation (22), we have:

$$\frac{\bar{\sigma}\ \tanh(\alpha\ l)}{\left\{\left(\dfrac{G_m}{G_I}-1\right)\ln\left(1+\dfrac{2t_I}{d_f}\right)+\ln\left(1+\dfrac{2t_m}{d_f}\right)\right\}^{1/2}}-Const \tag{A-1}$$

Substituting $t_m/d_f=1.0$ and $t_m/d_f=0.4$ into equation (A-1), and note that $\tanh(\alpha\ l)\approx1.0$, we have:

$$\frac{\overline{\sigma_{1.0}}}{(A+1.0986)^{1/2}}-\frac{\overline{\sigma_{0.4}}}{(A+0.5878)^{1/2}} \tag{A-2}$$

where

$\bar{\sigma}_{0.4},\ \bar{\sigma}_{1.0}$ = debonding stress of fiber/matrix interface corresponding to $t_m/d_f=1.0$ and $t_m/d_f=0.4$, respectively

$$A-\left(\frac{G_m}{G_I}-1\right)\ln\left(1+\frac{t_I}{r_f}\right) \tag{A-3}$$

Equation (A-2) can be rearranged as follows:

$$\left(\frac{G_m}{G_I}-1\right)\ln\left(1+\frac{t_I}{r_f}\right)-\frac{(1.0986-0.5878\ B)}{(B-1)} \tag{A-4}$$

where

$$B=(\bar{\sigma}_{1.0}/\bar{\sigma}_{0.4})^2 \tag{A-5}$$

For S-glass/epoxy, from reference 1:

$$\frac{\overline{\sigma_{1.0}}}{\sigma_{0.4}}-1.1$$

$$B-1.21$$

equation (A-4) becomes:

$$\left(\frac{G_m}{G_I} - 1\right) \ln\left(1 + \frac{t_I}{r_I}\right) - 1.8446$$

For graphite/epoxy, from reference 1:

$$\frac{\overline{\sigma_{1.0}}}{\sigma_{0.4}} - 1.092$$

$$B - 1.1924$$

equation (A-4) becomes:

$$\left(\frac{G_m}{G_I} - 1\right) \ln\left(1 + \frac{t_I}{r_I}\right) - 2.0672$$

INTERPHASE-SHEAR STRENGTH

From equation (28), the maximum interfacial shear stress can be written as follows:

$$\tau_{max} - \frac{\overline{\sigma}}{\sqrt{2}} \sqrt{\frac{G_m}{E_I}} \left\{\left(\frac{G_m}{G_0} - 1\right) \ln\left(1 + \frac{t_I}{r_I}\right) + \ln\left(1 + \frac{2t_m}{d_I}\right)\right\}^{-1/2} \qquad (A\text{-}6)$$

For S-glass fiber $G_m = 1.07$ GPA, $E_f = 86$ GPA from reference 1, for $t_m/d_f = 0.4$, $\overline{\sigma} = 777$ MPA, equation (A-6) becomes:

$$\tau_0 = 39 \text{ MPA}$$

For G_I/G_p, $G_m = 1.21$ GPA, $E_f = 241$ GPA, from reference 1, for $t_m/d_f = 0.4$, $\overline{\sigma} = 883$ MPA, equation (A-6) becomes:

$$\tau_0 = 27 \text{ MPA}$$

OUT-OF-DISPLACEMENT OF FIBER

From shear lag theory, the fiber axial displacement at $z = 0$ can be written as:

$$w - \frac{\overline{\sigma}}{E_f \alpha} \qquad (A\text{-}7)$$

where

$$\alpha = \frac{\sqrt{2}}{r_f} \sqrt{\frac{G_m}{E_f}} \left\{ \left(\frac{G_m}{G_l} - 1 \right) \ln\left(\frac{r_l}{r_f} \right) + \ln\left(\frac{r_m}{r_f} \right) \right\}^{-1/2} \tag{A-8}$$

For graphite/epoxy an $P = 1$ N, equation (A-7) becomes:

$$w = \frac{\bar{\sigma}}{E_f \alpha} = \frac{25.984}{241} \frac{1}{\alpha} = \frac{0.1078}{\alpha} \tag{A-9}$$

$$\alpha = 0.0286 \left\{ 2.0672 + \ln\left(1 + \frac{2 t_m}{d_f} \right) \right\}^{-1/2} \tag{A-10}$$

DEBONDING STRESSES

Graphite/Epoxy

From equation (A-1), we have:

$$\frac{\bar{\sigma}}{\left\{ 2.0672 + \ln\left(1 + \frac{2 t_m}{d_f} \right) \right\}^{-1/2}} = \frac{\sigma_{1.0}}{\{2.0672 + 1.0986\}^{1/2}}$$

After simplification, we have:

$$\bar{\sigma} = 542.36 \left\{ 2.0672 + \ln\left(1 + \frac{2 t_m}{d_f} \right) \right\}^{1/2}$$

σ vs. t_m/d_f is tabulated as shown in Table A-1.

S-glass/Epoxy

From equation (A-1) we have:

$$\frac{\bar{\sigma}}{\left\{ 1.8446 + \ln\left(1 + \frac{2 t_m}{d_f} \right) \right\}^{1/2}} = \frac{\overline{\sigma_{1.0}}}{\{1.8446 + 1.0986\}^{1/2}}$$

After simplification we have:

$$\bar{\sigma} = 498.375 \left\{ 1.8446 + \ln\left(1 + \frac{2 t_m}{d_f} \right) \right\}^{1/2}$$

σ VS. t_m/d_f is tabulated as shown in Table A-2.

Table A-1. $\bar{\sigma}$ vs. t_m/d_f for Graphite/Epoxy

t_m/d_f	$\bar{\sigma}_{Test}$ (MPA)	$\bar{\sigma}$ (MPA)	$E_{o/o}$
0.1	773.6	813.45	5.2
0.2	826.8	840.86	1.7
0.3	859.7	863.9	0.49
0.4	883.0	883.0	0.
0.5	902.9	901.09	−0.2
0.6	918.8	916.51	−0.25
0.7	932.5	930.37	−0.23
0.8	944.5	942.94	−0.17
0.9	955.3	954.4	−0.09
1.0	965.0	965.0	0.

Table A-2. $\bar{\sigma}$ vs. t_m/d_f for S-glass/Epoxy.

t_m/d_f	$\bar{\sigma}_{Test}$ (MPA)	$\bar{\sigma}$ (MPA)	$E_{o/o}$
0.1	673.0	709.5	5.4
0.2	723.0	736.0	1.8
0.3	754.0	758.2	.56
0.4	777.0	777.0	0.
0.5	795.5	793.92	−0.2
0.6	810.8	808.7	−0.26
0.7	823.9	821.95	−0.24
0.8	835.4	833.95	−0.17
0.9	845.7	844.92	−0.09
1.0	855.0	855.0	0.

FINITE ELEMENT ANALYSIS

From finite element analysis, for center fiber subjected to $\bar{\sigma} = 25,984.0$ MPA (i.e., P = 1 N), the computer outputs for interfacial shear, τ, and out-of-plane displacement, w, are shown in Table A-3.

Table A-3. Finite Element Results for P = 1 N ($t_i = .1\mu$m).

t_m/d_f	w (μm)	τ (MPA)
0.10	5.62	775.0
0.35	6.23	710.7
1.0	6.86	641.0

INTERPHASE SHEAR STRENGTH

Define the interphase shear stress at $\bar{\sigma} = 883$ MPA, which corresponds to the debonding stress of composite with $t_m/d_f = 0.4$ as interphase shear strength, then $\tau_0 = 704/25984 \times 883 = 23.9$ MPA.

DEBONDING STRESS $\bar{\sigma}$ vs. t_m/d_f

The debonding stress of composite for various t_m/d_f can be written as follows:

$$\bar{\sigma} = \frac{25984}{\tau^*} \times 23.9 \qquad \text{(A-11)}$$

where

τ^* = computer output of interphase shear stress corresponding to $\bar{\sigma} = 25984$ MPA.

Making use of data from Table A-3, we have the comparison of finite element results with the test results as shown in Table A-4.

Table A-4. Comparison of Debonding Stress
Between Test and Finite Element Analysis.

t_m/d_f	$\bar{\sigma}_{Test}$ (MPA)	τ^* (MPA)	$\bar{\sigma}$ MPA
0.1	773.6	775.0	801.3
0.35	874.2	710.7	874.2
1.0	965.0	641.0	969.2

OUT-OF-PLANE DISPLACEMENT

The comparison of out-of-phase displacement for shear lag theory and finite element analysis is shown in Table A-5. Shear lag solution is based on equations (A-9) and (A-10).

Table A-5. Comparison of Out-of-Plane Displacement Between
Shear Lag Theory and Finite Element Analysis.

t_m/d_f	w(μm) SHEAR LAG	w(μm) F.E.A.
0.1	5.653	5.62
0.2	5.84	—
0.3	6.004	—
0.4	6.075	6.23
0.5	6.2623	—
0.6	6.37	—
0.7	6.47	—
0.8	6.55	—
0.9	6.63	—
1.0	6.71	6.86

APPENDIX B: CALCULATION OF INTERPHASE SHEAR STRESS CONCENTRATION FACTOR AND MODE I FRACTURE ENERGY OF UNIDIRECTIONAL COMPOSITES

INTERPHASE SHEAR STRESS CONCENTRATION FACTOR, K_s

From equation (30) we have:

$$K_s = \frac{1}{\sqrt{2}} \frac{1}{\left\{ \left(\frac{G_m}{G_i} - 1 \right) \ln \left(1 + \frac{2t_i}{d_f} \right) + \ln \left(1 + \frac{2t_m}{d_f} \right) \right\}^{1/2}} \tag{B-1}$$

Equation (B-1) is used to calculate K_s for $t_m/d_f = 0.1$ and $t_m/d_f = 1.0$, respectively, as tabulated in Tables B-1 and B-2.

Table B-1. K_s vs. G_m/G_i for Various t_i/d_f ($t_m/d_f = 0.1$).

G_m/G_i	K_s		
	$t_i/d_f = 0.001$	$t_i/d_f = 0.005$	$t_i/d_f = 0.01$
1	1.66	1.66	1.66
10	1.58	1.36	1.17
10^2	1.15	0.65	0.48
10^3	0.48	0.22	0.16
10^4	0.16	0.1	0.05
10^5	0.05	0.02	0.02

Table B-2. K_s vs. G_m/G_i for Various t_i/d_f ($t_m/d_f = 1.0$).

G_m/G_i	K_s		
	$t_i/d_f = 0.001$	$t_i/d_f = 0.005$	$t_i/d_f = 0.01$
1	0.675	0.675	0.675
10	0.669	0.649	0.626
10^2	0.621	0.49	0.404
10^3	0.402	0.21	0.155
10^4	0.15	0.07	0.05
10^5	0.05	0.02	0.02

MODE 1 FRACTURE ENERGY OF UNIDIRECTIONAL COMPOSITE

From equation (29):

$$\bar{\sigma} = \frac{|\tau_{max}|}{K_s}\left\{\frac{E_f}{G_m}\right\}^{1/2} \tag{B-2}$$

The debonding stress of fiber/matrix interface can be written as follows:

$$\bar{\sigma} = \frac{\tau_0}{K_s}\left\{\frac{E_f}{G_m}\right\}^{1/2} \tag{B-3}$$

From equation (33):

$$g = \frac{\bar{\sigma}_0}{\sigma_{fu}} = \frac{\tau_0}{\sigma_{fu}K_s}\left\{\frac{E_f}{G_m}\right\}^{1/2} \tag{B-4}$$

For graphite/epoxy:

$$g = \frac{0.027}{2.5\,K_s}\left\{\frac{241}{1.21}\right\}^{1/2} = \frac{0.1524}{K_s} \tag{B-5}$$

where K_s can be obtained from equation (B-1) and Tables B-1 and B-2.

Table B-3. G_{INF}/C_{INF} vs. G_m/G_i for Various t_i/d_f ($t_m/d_f = 0.1$).

G_r/G_i	$t_i/d_f = 0.001$		G_m/G_i	$t_i/d_f = 0.005$		G_m/G_i	$t_i/d_f = 0.01$	
	g	$\overline{1-g+g^2-g^3}$		g	$\overline{1-g+g^2-g^3}$		g	$\overline{1-g+g2-g^3}$
1	0.092	0.9157	1	0.092	0.9157	1	0.092	0.9157
10	0.0965	0.912	10	0.112	0.90	10	0.1303	0.885
10^2	0.1325	0.883	10^2	0.235	0.810	10^2	0.3175	0.751
10^3	0.3175	0.751	10^3	0.693	0.455	10^3	0.9526	0.09
10^4	0.9526	0.09	2130	1.0	0.	1078	1.0	0.
10680	1.0	0.						

Table B-4. G_{INF}/C_{INF} vs. G_m/G_i for Various t_i/d_f ($t_m/d_f = 1.0$).

G_m/G_i	$t_i/d_f = 0.001$		G_m/G_i	$t_i/d_f = 0.005$		G_m/G_i	$t_i/d_f = 0.01$	
	g	$\dfrac{1}{1-g+g^2-g^3}$		g	$\dfrac{1}{1-g+g2-g^3}$		g	$\dfrac{1}{1-g+g2-g^3}$
1	0.2258	0.8137	1	0.2258	0.8137	1	0.2258	0.8137
10	0.2278	0.8123	10	0.2348	0.8074	10	0.2435	0.8014
10^2	0.2454	0.800	10^2	0.311	0.756	10^2	0.3772	0.7114
10^3	0.3791	0.71	10^3	0.72	0.425	10^3	0.98	0.
10^4	1.0	0.	2043	1.0	0.	1032	1.0	0.

THIS PAGE INTENTIONALLY LEFT BLANK

DISTRIBUTION LIST
Report No. NADC-90001-60

No. of Copies

Defense Technical Information Center 2
ATTN: DTIC-FDAB
Cameron Station BG5
Alexandria, VA 22304-6145

Center for Naval Analysis 1
4401 Fort Avenue
P.O. Box 16268
Alexandria, VA 22302-0268

Office of Naval Research 2
Washington, DC 20350

Naval Air Development Center 17
Warminster, PA 18974-5000
    (5 for Code 6043; H. Tsai)
    (5 for Code 6043; A. Arocho)
    (5 for Code 6043; L. Gause)
    (2 for Code 8131)